Morphological analysis of brain injury after early neonatal hypoxia - ischemia in mice

Borden, Gabriel David

UNIVERSITY OF ZAGREB

SCHOOL OF MEDICINE

Gabriel Borden

Morphological Analysis of Brain Injury after Early Neonatal Hypoxia - Ischemia in Mice

Graduate Thesis

Zagreb, 2016

This graduate thesis was made in the Department of Histology and Embryology School of Medicine Zagreb University and at the Laboratory for Regenerative Neuroscience and the GlowLab Multimodal Imaging Facility, mentored by Dr. sc. Marina Dobrivojević and was submitted for evaluation in 2016.

ABBREVIATIONS

CCA - common carotid artery

CP - cerebral palsy

DWI – diffusion weighted imaging

Gd - gadolinium

GFAP - glial fibrillary acidic protein

HI – hypoxia - ischemia

MR - magnetic resonance

NeuN - "neuronal nuclei"

OL - oligodendrocyte

PND – postnatal day

PVL - periventricular leukomalacia

RV - Rice-Vannucci

SNR – signal to noise ratio

T2WI - T2-weighted imaging

CONTENTS

1 SUMMARY

Morphological Analysis of Brain Injury after Early Neonatal Hypoxia - Ischemia in Mice

Gabriel Borden

Perinatal ischemia is a common cause of cerebral palsy and other human morbidity. It is a growing problem in preterm infants in whom it is increasingly common because modern standards of care result in a greater number of infants who survive prematurity to experience ischemic brain pathology. In excess of 50% of babies born at 24 weeks currently enjoy long-term survival. Many neurodevelopmental processes in newborn mice correspond to this period in human development. Towards a better model of hypoxic/ischemic events in early human premature parturition, an implementation of the Rice-Vannucci model of perinatal ischemia in zero day old mice is therefore presented herein. The Rice-Vannucci (RV) model entails unilateral ligation of the common catid artery followed by a period of relative hypoxia, applied to neonatal rats or mice. Previously the youngest animals reported with this model were three day old mice, and one day old rats. Towards a better model of hypoxic-ischemic events in early human premature parturition, an implementation of the Rice-Vannucci (R-V) model of perinatal ischemia in zero day old mice is therefore presented herein. The modifications of the RV model entail unilateral ligation and interruption of the common carotid artery followed by a period of relative hypoxia, applied to postnatal day zero mice. Multiple imaging modalities were employed in the analysis, including magnetic resonance imaging (MRI), histological Nissl staining, as well as immunohistochemical staining of *ex-vivo* day three and seven postnatal mice brains. Together, comparing diffusion-weighted and T2-weighted MRI to Nissl staining data confirm the successful implementation of the R-V model, establishing a foundation for follow-up investigations.

Keywords: perinatal ischemia, Rice-Vannucci, neonatal

2 PREFACE

Every year, in the United States alone, an estimated 500,000 babies are born preterm, by definition before completing 37 weeks of gestation (Buhl et al. 2010). Medical progress in neonatology has significantly improved survival statistics, particularly for very early preterm infants, but a significant subset suffers long-term morbidity from suboptimal neurodevelopmental outcomes (Lawn et al. 2005). Cerebral injury in a disproportionately high percentage of the survivors of premature birth is associated with hypoxic-ischemic brain injury (Volpe 1996). Hypoxic-ischemic brain injury may result in cerebral palsy (CP), mental retardation, or learning disabilities (Robertson & Finer 1985). The incidence of CP increases dramatically with the decline in gestational age at birth, with a prevalence of 2 to 4 per 1000 births and rising even higher with birth weight lower than 1000 g (Schmidt et al. 2001). While the exact causes of hypoxic-ischemic injury are unknown, a variety of intrapartum conditions as placenta issues, maternal blood pressure problems, maternal uterine rupture, and umbilical cord complications have been linked to hypoxic-ischemic brain injury (Badawi et al. 1998).

Periventricular leukomalacia (PVL) is one of the most common pathological causes of CP which is characterized by focal necrosis or diffuse injury of the white matter. Among potential mechanisms underlying diffuse PVL, the most studied is pre-oligodendrocyte (pre-OL) injury which leads to serious impairment of axonal myelination specifically affecting the subplate neurons which have a crucial role in the development of the cerebral cortex and deep nuclei (Du & Dreyfus 2002, Dai et al. 2003). Hypoxia-ischemia (HI) causes selective subplate neuronal death and disrupts normal cortical development, resulting in plasticity impairments along with damage to the thalamus leading to pronounced white matter axon damage and gliosis (McQuillen et al. 2003, McQuillen & Ferriero 2005, Ranasinghe et al. 2015). In humans, susceptibility to white matter injury appears between 23 and 32 weeks of gestation due to the higher energy needs of the brain while supporting the rapid brain growth, making oxygen and blood supply more critical (Semple et al. 2013, Marin-Padilla 1997, Mifsud et al. 2014). Different studies have shown a link between myelination impairment and abnormal OL differentiation processes originating during susceptibility windows prior to the beginning of myelination (Back et al. 2001, Yuen et al. 2014, Buser 2012, Back & Miller 2014). To facilitate the understanding of susceptibility to white matter injury comparative timetables

between human and other species for the various developmental stages have been proposed, but direct comparison of brain development between human and other species are not perfect and differ between studies suggesting that the maturation peak of OL occurs at PNDs 1-5 (Marin-Padilla 1997, Dunn 1995, Craig et al. 2003, Dean et al. 2011).

The crucial aspect in determining the response to an insult is the developmental stage. Insults occurring at different time points differ in consequences, from those occurring in the first trimester which are linked to abnormal cerebral development, to those occurring in the late second and early third trimester which lead to periventricular white matter injury associated with neuronal abnormalities, while late third trimester damage is associated with cortical and deep gray matter lesions (Krageloh-Mann & Cans 2009). Some studies also suggest sex differences in response to developmental brain injury, for instance, preterm males showed greater vulnerability to white matter damage than female of the same age (Johnston & Hagberg 2007).

Neonatal hypoxia-ischemia is associated with significant damage to both grey and white matter leading to major behavioral and neuroanatomical morbidity. Different therapeutic strategies are still under study since preterm and early preterm infants react differently than term infants, for example therapeutic hypothermia is a standard of care procedure for term infants, however it is not recommended in preterm infants due to potential collateral damage, such as intra-cerebral hemorrhage (Jacobs et al. 2007, Thoresen 2015). Since clinical trials testing therapeutic strategies undergo various hardships defining recruitment criteria, mainly due to the heterogeneous patient population or inadequate group sizes, the need for adequate animal models is of great importance. Variations of the first model, the classical Rice-Vannucci model have been employed in the study of perinatal ischemia for over 30 years since the procedure was originally described (Rice et al. 1981).

2.1 The Rice-Vannucci model

The Rice-Vannucci model is an adaptation of the Levine model of HI in adult rats using postnatal day 7 (PND7) neonatal rats, equivalent to term or near term human infants (Clancy et al. 2007). In the original report, 7 day old rats were subjected to unilateral common

carotid artery ligation followed by a period of relative hypoxia, reliably producing histologically apparent pathology concentrated in the ipsilateral hemisphere. The injury induced in this model can be observed in only 56% of the animals, suggesting a variability of the technique, and is described as a spectrum, ranging from "moderate" to "severe." The injury affects the cerebral cortex, the basal ganglia and thalamus, the subcortical and periventricular white matter, and the hippocampus which depends on the severity of the HI insult (Rice et al. 1981, Clancy et al. 2007, Vannucci & Hagberg 2004, Vannucci & Vannucci 2005). In its original form, the Rice-Vannucci model was intended to inform ischemic insults to full term human infants during or just prior to parturition. However, studies have shown that the Rice-Vanucci model does not mimic the human condition optimally, since the white matter development in PND7 rats and the type of injury produced are not similar to that in humans. In most cases in the infant brain the lesion in comprises diffuse apoptotic and relatively small necrotic areas, while the Rice-Vannucci model shows severe injury with multiple lesions involving both white matter and gray matter (Rice et al. 1981, Khwaja & Volpe 2008, Volpe 2001, Vannucci et al. 1999).

2.2 Optimization of the Rice-Vanucci model

One of the first modifications of the HI model was done in rats at PND1 at a developmental stage comparable to the human brain in the last trimester of gestation (Sheldon et al. 1996). At PND1 rat brain damage comprised neuronal loss, white matter thinning, and activation of microglia and macrophages (Sheldon et al. 1996). A few years later a bilateral common carotid artery occlusion (BCAO) model in Wistar rats at PND5 with no subsequent hypoxia was developed; this model aims to mimic the ischemic reduction of the cerebrospinal fluid flow which results in white matter loss (Uehara et al. 1999). Since other researchers have failed to reproduce consistent results with the original BCAO model, a modification entailing temporary bilateral ligation of common carotid arteries along with hypoxia in PND7 rat pups saw developed, which inflicted a greater degree of damage (Jelinski et al. 1999). Different attempts to generate a reliable model of white matter injury producing less severe brain damage were attempted by changing the time of hypoxia, percent of oxygen or changing the temperature applied during hypoxia (Follett et al. 2000). For example, it has been shown that

applying mild hypothermia during hypoxia significantly reduces brain damage in PND7 rat pups (Yager et al. 1993).

Subsequent authors have extended the model to mice while working to define strain differences, obtain reproducibility and standardized degrees of brain damage. As different strains of mice were compared it was found that the 129Sv strain was highly resistant to injury while displaying very high mortality, compared to CD1 which showed brain susceptibility with little mortality rate (Sheldon et al. 1998). C57Bl/6 mice show an intermediate degree of suitability to the model. As more research using the HI model was undertaken different authors were successful in producing consistent mild brain damage using animals of different ages, from PND3 to PND5 (Nijboer et al. 2007). Gender differences were also elucidated as arising from pathophysiological events underlying HI, specifically that HI-induced cell death is mediated by the caspase-3 pathway in females, but not in males (Chen et al. 2011).

As rising standards of preterm infant care have increased the survival rate of neonates born ever more prematurely, the need to model ischemia in this vulnerable population has also grown. In parallel with this progress in treatment there has also been an increase in the absolute proportion of infants born after fewer than 37 weeks of gestation; in the USA the rate grew from 9.4% in 1981 to 12.5% in 2005 (Behrman 2007). Additionally, sophisticated comparative developmental models have extrapolated events in the organization of the central nervous system between species in a more detailed way. For example a new neuroinformatics approach was developed upon the observation of up to 102 neurodevelopmental events in 10 different species (Clancy et al. 2007). These numerous developmental milestones do not always map between species in a temporally linear manner. Hypoxia–ischemia rodent models use rodents PND2-3 to produce brain injury at aproximately similar stage of cellular development as for 24 to 32 weeks of gestation in human. At these time points, cells from the OL lineage were shown to be maximally vulnerable to hypoxic–ischemic injury (Rumajogee et al. 2016). However, despite the similarity of cellular stage development, there is a vast difference in structural development particularly for the cerebral cortex with considerably longer neurogenesis in humans (Kornack & Rakic 1998). Moreover, the subplate, a region vulnerable to hypoxic–ischemic injury, has a more complex function in the formation of

human cortex pathways than in rodents, with concomitant increase in structural complexity and relative size. The time course of development also differs considerably between species with regard to the subplate, reaching its complete structure by E16–18 compared to 24–32 weeks of gestation in humans (Kostovic & Rakic 1990, Wang et al. 2010). Thus to model different human developmental phenomena, and different expressions of human pathology resulting from perinatal ischemia, rodents of different corresponding ages should ideally be studied.

Although there are a wide variety of animal studies demonstrating the effects of neonatal HI injury there are no studies using PND0 mice, which we chose according to the website *Translating Time* (introduced in Clancy et al. 2007), where PND0 is within the window comparable to human early prematurity. Furthermore after implementing modifications to the established Rice-Vannucci framework in PND 0 mice, we explored if magnetic resonance imaging (MRI) could be used as a valuable method for assessment of early temporal changes after HI in the *ex vivo* neonatal mice brain. MRI provides a wide range of diagnostic markers for the detection of human as well as for rodent models of neonatal HI (Ment et al. 2002). Diffusion weighted and T2-weighted MRI have been used to study edema formation after HI, along with diffusion tensor imaging used to assess changes in white matter following HI (Wendland et al. 2008, Aden et al. 2002, Ten et al. 2004, Wang et al. 2008). However, due to a lack of specific MR contrasts that can delineate neuronal damage, detailed examination of pathophysiological changes induced by HI still mostly relies on post-mortem histology.

3 HYPOTHESIS

The Rice-Vannucci model can be extended to mice younger than previously published (PND3) to provide a useful model of perinatal ischemia early preterm infants; an ex-vivo MR scanning protocol can be developed and verified by histology which can identify the pathology arising from the model.

4 OBJECTIVES

The main objective of this thesis was to establish a postnatal day zero neonatal mouse model of hypoxic-ischemic brain injury and subsequently verify this model by developing a new protocol for ex-vivo magnetic resonance imaging along with classical histological tissue staining. In order to achieve the main objective specific sub-objectives were set:

1.) To implement the Rice-Vannucci hypoxic-ischemic model in postnatal day zero neonatal mice.
2.) To develop a magnetic resonance imaging protocol for the visualization of the pathological changes in early neonatal ex-vivo brains.
3.) To confirm magnetic resonance images with histological and immunohistochemical methods.

5 METHODS

5.1 Animals

All experiments were carried out on neonatal inbred strain CD1 mice pups at postnatal day 0 (PDN0), bred and housed in the animal facility at the Croatian Institute for Brain Research (Table 1). Dams were housed under 12:12 hour light/dark cycle with food and water ad libitum. All animal procedures were approved by the Internal Review Board of the Ethical Committee of the School of Medicine, University of Zagreb, and were in accordance with the Ethical Codex of the Croatian Society for Laboratory Animal Science. All experiments were carried out in accordance with the EU Directive 2010/63/EU on the protection of animals used for scientific purposes.

Table 1. Animals used for this study.

Animal Number	Age at Surgery/Hypoxia	Age at Sacrifice	Minutes at 5% O2	Surgery	Gender
1	PND0	PND3	0	sham	F
2	PND0	PND3	0	sham	M
3	PND0	PND3	0	sham	F
5	PND0	PND3	0	CCA lig.	M
6	PND0	PND3	20	CCA lig.	M
7	PND0	PND3	20	CCA lig.	F
8	PND0	PND3	20	CCA lig.	F
9	PND0	PND3	20	CCA lig.	M
10	PND0	PND7	20	CCA lig.	M
11	PND0	PND7	20	CCA lig.	M
12	PND0	PND7	20	CCA lig.	M
13	PND0	PND7	20	CCA lig.	F
14	PND0	PND7	0	sham	F
15	PND0	PND7	0	sham	F

Figure 1. A zero-day old pup, shown with an American penny for scale. The common carotid artery has a diameter of approximately 200 μm at this age.

5.2 Modification of the Rice-Vanucci model

To acclimate the dam to the smells associated with handling, paper pieces impregnated with the smell of the products used during experiments were placed in the cage several days prior to surgery (Libbin 1979). Also, prior to removal and immediately after return of pups from their cage for surgery, the dams were briefly introduced to isoflurane anesthesia. Great care was taken not to touch the pups without clean gloves, and to disinfect the surfaces the pup may contact during the procedures. When surgery was performed on one pup, all pups from the litter were removed from the cage and placed in a pre-warmed chamber immersed in

a water bath maintained at 37 degrees C. Immediately following the procedure, the pup that underwent surgery was allowed to recover in the chamber until it was fully mobile. The pup was then gently rubbed with the bedding from the home cage and returned to the home cage with the rest of the litter. This reduced the rate of rejection or maternal cannibalism by the dam.

Anesthesia was induced with 4% isoflurane in oxygen and kept at 1.5% for maintenance. The mice pup was placed on a heating pad which ensured temperature maintenance at 37 degrees C during the entire procedure. Following anesthesia induction, a small incision was made to the left of the midline, and the glands overlying the large neck vessels gently deflected with a cotton swab. Next, a small tear in the overlying sheet of muscle was made using a pair of Dumont #5 extra fine forceps (Figure 2). Then fine Dumont #7 curved forceps were inserted through the tear and under the common carotid artery (CCA; Figure 3) and a single ~3cm length of 6-0 silk suture was then drawn underneath by grasping the suture in its middle portion. The silk suture was then cut to yield two ligatures which are subsequently tied and trimmed. (Figure 4). The section of CCA between the ligatures is then cut with a small Vannas scissors, and the glands gently returned to the neck pocket before closing the wound. The skin bordering of the wound was covered with a small quantity of Newskin® (Prestige Brands, Tarrytown, NY, USA) using the supplied brush applicator (Figure 5). A precut rectangle of single-ply sterilized tissue is then overlaid. More Newskin® was applied at the corners as necessary. This technique was found to reduce subsequent mortality relative to conventional suturing, most likely by discouraging maternal cannibalism.

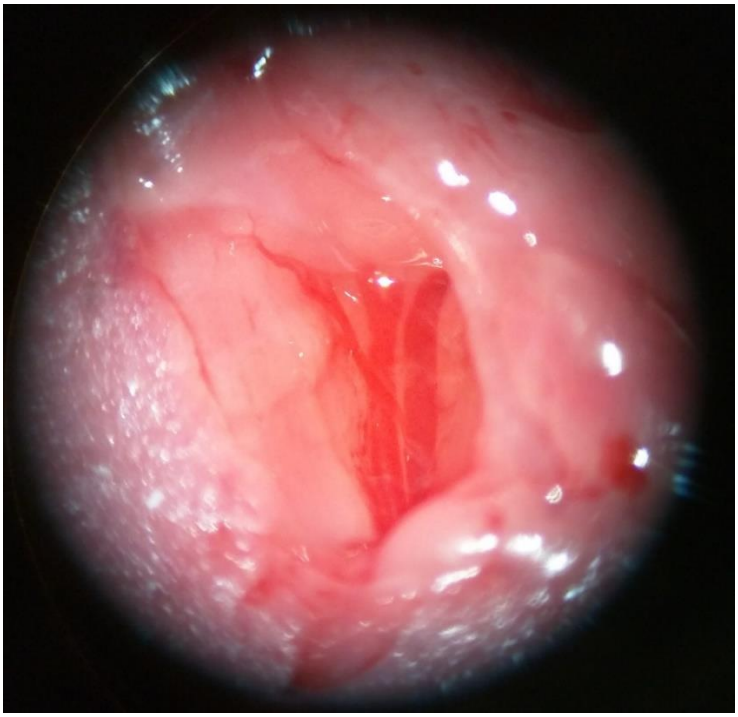

Figure 2. Photograph showing the common carotid artery (CCA) on the left and the external jugular vein on the right. Often, the small vessel overlies the CCA as seen here and must be carefully avoided.

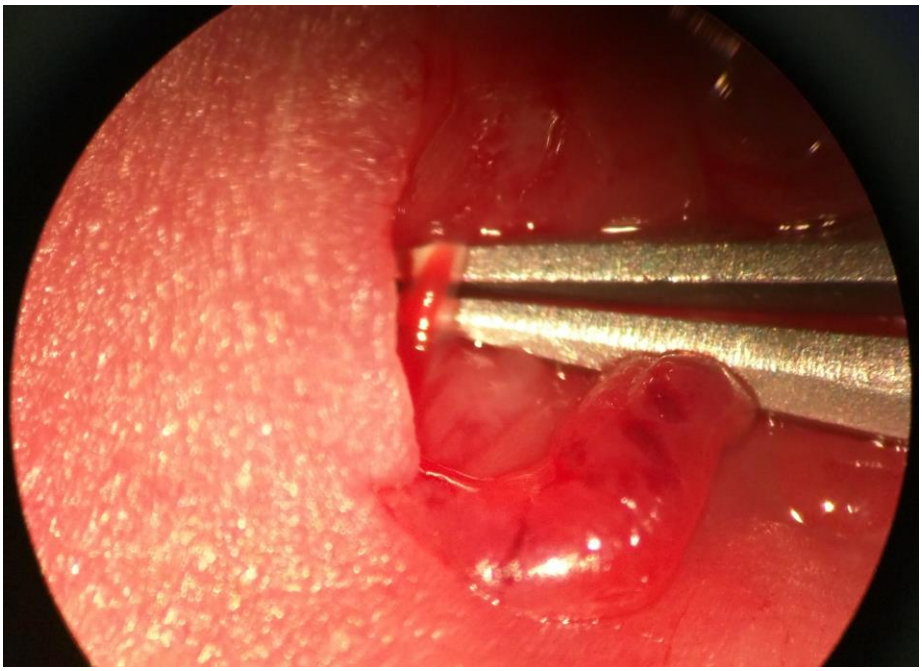

Figure 3. Photograph of the common carotid artery (CCA). Capture of the artery can be confirmed by observing the pulsation of blood through the lumen while the deflecting force and tension are low.

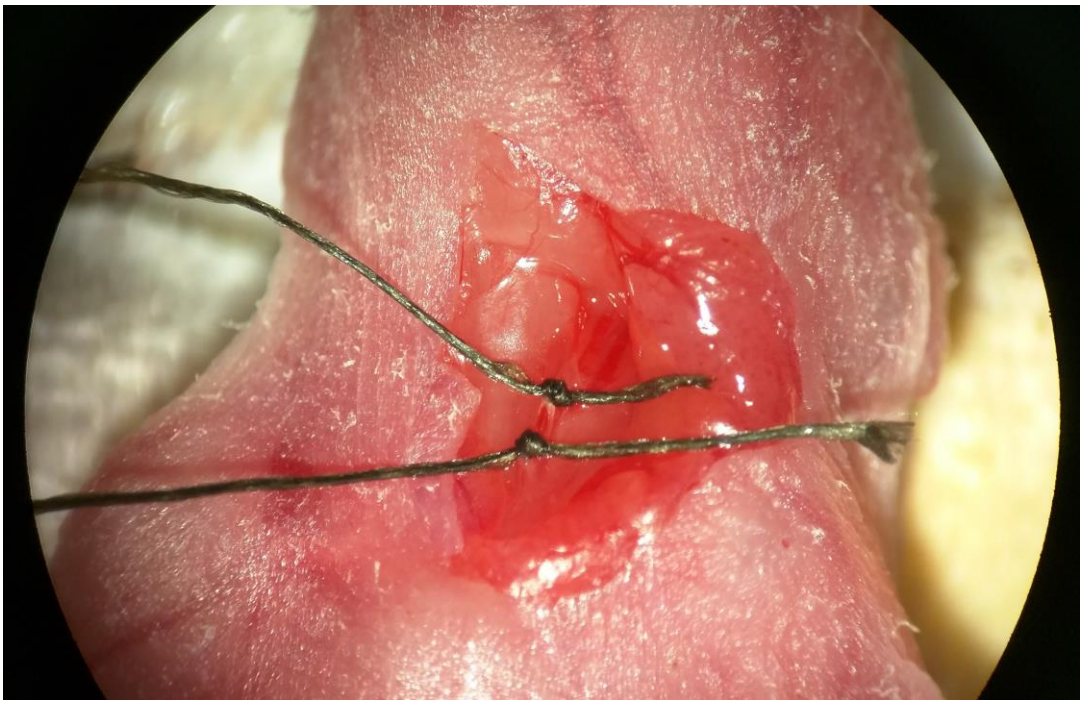

Figure 4. The common carotid artery (CCA) is shown here after the tying of the sutures, just prior to division.A single ~3cm length of 6-0 silk drawn underneath the CCA by grasping the suture in its middle portion and then cut to yield two ligatures which are subsequently tied and trimmed with a small Vannas scissors.

Figure 5. Wound closure using Newskin®. The skin bordering the surgical wound was covered with a small quantity of Newskin® (Prestige Brands, Tarrytown, NY, USA) and a precut rectangle of single-ply sterilized tissue.

In sham operated animals, following anesthesia induction, a small incision was made to the left of the midline, and the glands overlying the large neck vessels gently deflected with a cotton swab. Next, a small tear in the overlying sheet of muscle was made using a pair of Dumont #5 extra fine forceps but the CCA was not sutured and cutted. The glands were then gently returned to the neck pocket before closing the wound covering it with Newskin and of sterilized tissue.

Immediately following the surgical procedure, the pup that underwent surgery was allowed to recover in the chamber until it was fully mobile and then transferred to a pre-warmed hypoxic chamber. The chamber was modified to contain a Grove O2 gas sensor (Seeed Technology Inc., Shenzhen, China) which was connected to an Arduino Mega 2580

(Arduino, Turin, Italy) electronic prototyping board via a ribbon cable threaded through the gas outflow tubing. This Arduino board was connected to a small laptop computer from which a simple program based on the C/C++ programming language was uploaded (Table 2), which enabled the O2 concentration to be monitored via the computer.

Inside the hypoxic chamber, the pups were placed in a pre-sterilized container lined with sterilized paper to absorb any urine produced, in order to prevent possible aspiration (Figure 6). After the experimental animals were sealed inside, the chamber was flushed with N_2 until the O_2 concentration was reduced to 5%, and confirmed to be stable at within 0.2% of this value. The chamber was then disconnected, closed, and placed in a cell culture incubator maintained at 37 degrees C. After the hypoxic interval, the chamber was removed and reconnected to confirm that the concentration of O_2 was unchanged. The use of a sealed container was justified via the following calculation: PND0 old mice consume approximately 1.75mL of O_2 per gram per hour (Fitzgerald 1953). The long term value of the respiratory exchange ratio (RER), relating carbon dioxide production to oxygen consumption varies between 0.7 and 1 depending on the energy source (it can slightly exceed 1 but only for brief periods of intense exertion). Since each PND0 pup weighs approximately 1.4g, a reasonable upper bound on oxygen consumption for a group of 20 pups for a half hour period would therefore be 24.5mL. Since these reference respiratory data were established under normoxic conditions, our animals should consume less in a 5% O_2 environment. Given that the chamber used has a volume of approximately 12cm x $20cm^2$ x $\pi \approx$ 15,000mL of which the 5% O_2 portion is 750mL, consumption of 24.5mL would only lower the O_2 % to 4.8%, a difference unlikely to lead to significantly different physiological consequences than 5%. In agreement with this reasoning, our actual measurement of the O_2 differed by no more than 0.1% (the limit of detection for our equipment) between the beginning and end of any hypoxic interval conducted. Similarly, the carbon dioxide content of the chamber could be expected to rise from 0.04% of normal air at the beginning of the experiment to at most 0.19% assuming an RER of 0.9. Workplace exposure guidelines for CO_2 are commonly placed at 0.5% (5000 ppm). Thus there seems to be no possibility of complicating effects from the use of a sealed chamber with our experimental parameters.

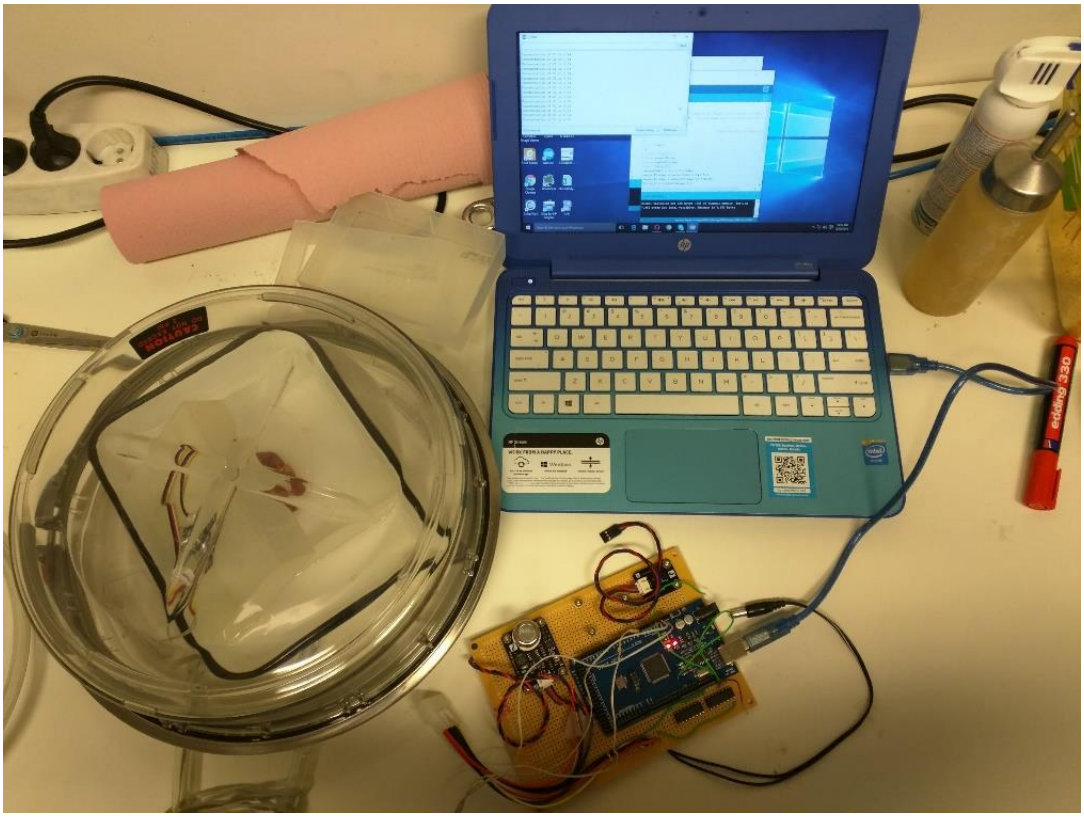

Figure 6. The hypoxic chamber setup being partially flushed with pure N_2. The tray containing the pups is itself floating in a larger container containing a few millimeters of water to humidify the atmosphere in the chamber and improve temperature stability while loading and unloading.

Overall, mortality from the procedure ranged from 20 to 50%, with most losses occurring during hypoxia or in the ensuing 24 hours. Operative mortality was typically under 5%; most losses occurred during, or in the 24 hours following, hypoxia.

Table 2. Arduino Code Listing for Grove O2 Gas Sensor

```
        // test Grove - Gas Sensor(O2)
      float  VoutArray[]  =    {  0.30769  ,20.00000,  40.00000  ,60.00000  ,120.61538
,186.76923};
      float  O2ConArray[] =  { 0.00018, 2.66129, 5.32258, 8.05300, 16.19851, 25.15367};

      void setup() {
        // put your setup code here, to run once:
        Serial.begin(9600);
```

```
}

void loop() {
  // put your main code here, to run repeatedly:

  Serial.print("Vout =");
  Serial.print(readO2Vout(A0));
  Serial.print(" V, Concentration of O2 is ");
  Serial.println(readConcentration(A0));

  delay(500);

}

float readO2Vout(uint8_t analogpin)
{

    // Vout samples are with reference to 3.3V
    float MeasuredVout = analogRead(A0) * (3.3 / 1023.0);
    return MeasuredVout;

}

float readConcentration(uint8_t analogpin)
{


    // Vout samples are with reference to 3.3V
    float MeasuredVout = analogRead(A0) * (3.3 / 1023.0);
    float Concentration = FmultiMap(MeasuredVout, VoutArray,O2ConArray, 6);
    float Concentration_Percentage=Concentration*100;


/*****************************************************************************

    The O2 Concentration in percentage is calculated based on wiki page Graph


    The data from the graph is extracted using WebPlotDigitizer
    http://arohatgi.info/WebPlotDigitizer/app/

    VoutArray[] and O2ConArray[] are these extracted data. Using MultiMap, the data
    is interpolated to get the O2 Concentration in percentage.
```

```
            This implementation uses floating point arithmetic and hence will consume
            more flash, RAM and time.

            The O2 Concentration in percentage is an approximation and depends on the accuracy of
            Graph used.


**********************************************************************************/

            return Concentration_Percentage;
          }


          //This code uses MultiMap implementation from http://playground.arduino.cc/Main/MultiMap

          float FmultiMap(float val, float * _in, float * _out, uint8_t size)
          {
           // take care the value is within range
           // val = constrain(val, _in[0], _in[size-1]);
           if (val <= _in[0]) return _out[0];
           if (val >= _in[size-1]) return _out[size-1];

           // search right interval
           uint8_t pos = 1;  // _in[0] allready tested
           while(val > _in[pos]) pos++;

           // this will handle all exact "points" in the _in array
           if (val == _in[pos]) return _out[pos];

           // interpolate in the right segment for the rest
           return (val - _in[pos-1]) * (_out[pos] - _out[pos-1]) / (_in[pos] - _in[pos-1]) + _out[pos-1];
          }
```

5.3 MR Imaging

5.3.1 MR Optimization

To maximize contrast, T1 and T2 relaxation curves (with RareVTR and MSME sequences, respectively) were measured and plotted for cortex, striatum, ventricle and

hippocampus in a series of optimization studies of several PND3 brains from mice which were soaked in different concentrations of Omniscan (GE healthcare, Waukusha, WI, USA) for 4 days. Once an optimal concentration was determined, T1 and T2 maps were again obtained using both PND3 and PND7 brains from the study series before proceeding. TR and TE values for T2 scans were calculated by plotting relaxation curves for the tissues sampled in Matlab (MathWorks, Natick, MA, USA) and identifying parameter values that resulted in greater than approximately 15% contrast between the lightest and darkest regions.

5.3.2 MR Scans

After initial optimization studies, brains were soaked in 0.5mM Omniscan for 4 days. Subsequently they were immersed in Fomblin (Solvay, Brussels, Belgium) for 1-2 days before scanning in a 1.8ml freezer tube, held in place with a custom cut piece of sponge (Figure 7).

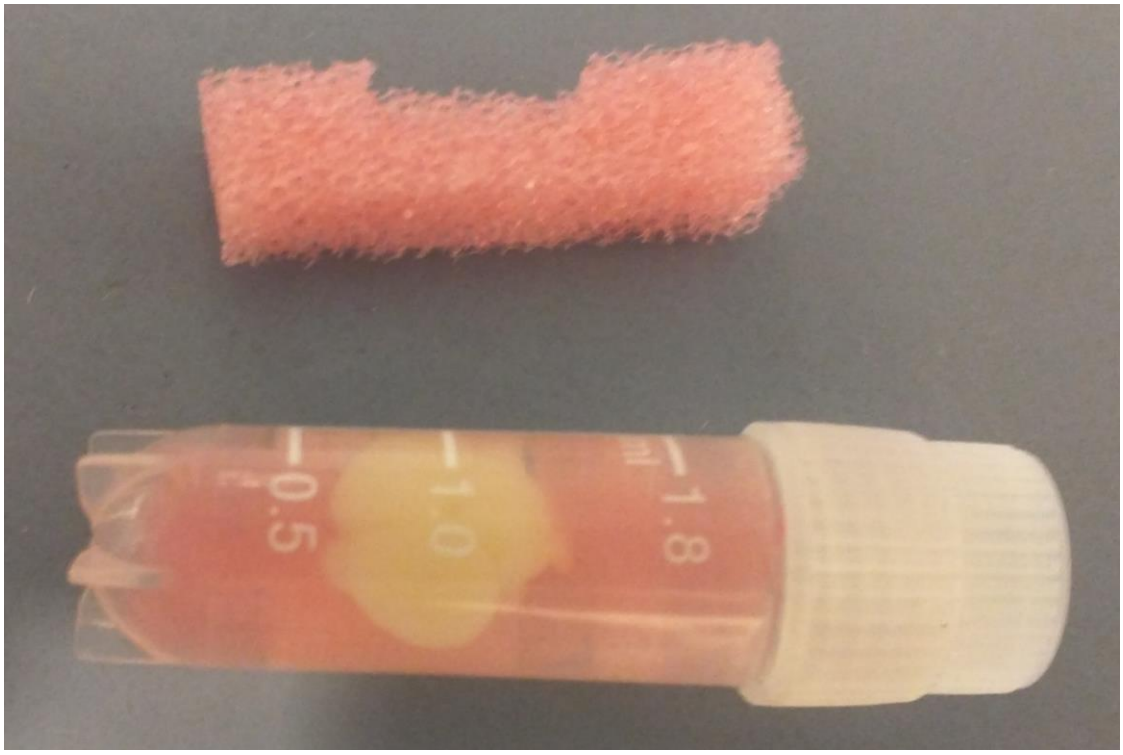

Figure 7. Preparation for MRI scanning. The brain is immersed in Fomblin and held in place with a specially cut piece of sponge.

Scans were performed on a 7T Bruker BioSpec 70/20 USR preclinical MRI system (Bruker Corporation, Billerica, MA, USA), using an 86mm volume resonator transmit coil and a 2-channel surface mouse brain receiver coil. For both time points (PND3 and PND7), both T2-weighted and diffusion-weighted scans were obtained.

5.3.3 PND3 MR image acquisition

For PND3 brains the T2-weighted imaging (T2WI) scans employed a multi-slice, multi-echo protocol with repetition time (TR) = 2200 ms, echo time (TE) = 84 ms (effective; average of 2 echoes), with fat suppression activated, constructed from 48 averaging. Geometrically, the scan consisted of 12 slices with a field of view of 12x6 mm and an image size of 160x80 pixels, corresponding to an in-plane resolution of 75x75 microns. The total scan time was 1 hour and 45 minutes.

Geometrically, the diffusion weighted imaging (DWI) scans for the PND3 series were unchanged from the T2-weighted parameters consisting of 12 slices with a field of view of 12x6 mm and an image size of 160x80 pixels, corresponding to an in-plane resolution of

75x75 microns. Fat suppression was turned off, TR set to 1800 ms with a TE = 18.5 ms with 24 averages. Diffusion specific parameters comprised a spin echo preparation, a gradient duration of 2.6 ms, gradient separation of 9.6 ms, one diffusion direction, max b-value of 1687 s/mm^2 and b-value of 1300 s/mm^2. Total scan time for PDN3 diffusion scans was 1 hour and 26 minutes.

5.3.4 PND7 MR image acquisition

The scan parameters for PND7 brains were similar to those for PND3 brains, with the following differences: For the T2-weighted scans, TR = 2600 ms, TE = 81 ms (with an average of two echoes) with 15 slices, to account for the larger brain size at PND7, resulting in a scan time of 2 hours and 15 minutes. For the diffusion weighted spin-echo sequence for PND7 animals, scanning parameters changed from the PND3 series were the following: TR = 1200 ms, TE = 18.5 ms, with 15 slices, for a total scan time of 57.5 minutes.

5.4 Tissue Processing and Histology

Following sacrifice by decapitation, the brains of PND3 animals were removed from their skulls and placed in 4% paraformaldehyde for at least 48 hours. PND7 brains were handled similarly, but after animals were transcardially perfused with phosphate buffered saline and 4% paraformaldehyde.

Prior to cryosectioning, brains were soaked in 30% sucrose for at least 48 hours and then imbedded in Tissue-Tek O.C.T. compound, (Sakura, Tokyo, Japan). Sectioning was performed on a Leica CM 1850 (Leica Biosystems, Wetzlar, Germany). 25 micron sections were then mounted on Superfrost Plus slides (Thermo Fisher Scientific, Inc., Waltham, MA, USA).

5.4.1 Nissl Staining

Every fourth section was used for Nissl staining procedure. Sections were fixed in 100% methanol for 10 minutes, and further rehydrated in a series of decreasing alcohol baths (95% ethyl alcohol [EtOH] 15 min, 70% EtOH 2 min, and 50% EtOH 2 min), rinsed twice in distilled water for 2 minutes and stained with Cresyl Violet stain for 6 minutes. After staining, sections were rinsed twice in water for 2 minutes and afterwards dehydrated in a series of

increasing alcohol baths (50% EtOH 2 minutes, 70% acidic EtOH [1% glacial acetic acid in 70% EtOH] 2 minutes, 95% EtOH 2 minutes, 95% EtOH a few dips, and 100% EtOH 1 minutes). The slides were coverslipped with with Biomount (BioGnost, Zagreb, Croatia). Slides were dried overnight. Brain sections were examined under a light microscope and photographed under 10× and 40× magnification on both ipsilateral (ischemic) and contralateral side and also digitized using a Flatbed Epson perfection 4870 photo scanner (Epson America, Inc., Long Beach, CA, USA), with a resolution of 4800 dpi.

5.4.2 Immunohistochemistry

For fluorescent immunohistochemistry, cryostat 25 μm-thick coronal sections were rinsed in PBS 4 times for 5 minutes in order to remove the O.C.T. compound. Sections were blocked for 30 minutes in 0.1 M PBS containing 10% goat or donkey serum, depending on the species used to produce the corresponding secondary antibody and 0.25% Triton X-100. Incubation with anti-cleaved caspase-3 (1:600, Cat. No. Asp175, Cell Signaling Technology, Danvers, MA, USA) and anti-NeuN (1:300, Cat. No. MAB377, EMD Millipore Corp., Billerica, MA, USA) was performed overnight at room temperature in PBS buffer containing 1% goat serum and 0.25% Triton X-100 (both Sigma Aldrich). Control slices were incubated overnight in a buffer that was not containing primary antibody. Slices were rinsed with PBS containing 0.25% Triton X-100 4 times for 5 minutes. Next, slices were incubated for 2 hours at room temperature in goat anti-mouse Alexa 488 secondary antibody (Thermo Fisher Scientific, Inc., Waltham, MA, USA) at 1:500 dilution. After incubation, slides were washed with PBS containing TritonX-100, stained with DAPI (4',6-diamidino-2-phenylindole, 1:8000), then coverslipped, mounted with Dako Mounting Medium (Dako A/S, Glostrup, Denmark) and left overnight to dry. Brain sections were examined under a fluorescence microscope and photographed under 40 × magnification on both, ipsilateral (ischemic) and contralateral side.

5.5 Sex Determination via Genotyping

For all animals too young to be easily sexed by inspection, tail tips were collected prior the time of sacrifice. DNA was purified from these samples and genotypes determined by PCR as detailed previously (Clapcote & Roder, 2005). Briefly, DNA from the samples was

amplified for 35 cycles on an Applied Biosystems 2720 Thermal Cycler using the forward primer sequence 5'-CTGAAGCTTTTGGCTTTGAG-3' and reverse primer sequence 5'-CCACTGCCAAATTCTTTGG-3' (Thermo Fisher Scientific, Inc., Waltham, MA, USA), and electreophoresed on agarose gel, yielding a single 331bp band for females, and two bands of 302 and 331bp for males. The method was verified to be accurate on adult animals of known gender. Two samples, from animals 2-4 and 2-12, did not yield definitive results from the initial run. A more diluted quantity of DNA from these two samples was amplified again, at a slightly lower annealing temperature, 53°C, and for 40 cycles, which gave conclusive results.

6 RESULTS

6.1 MR Imaging

6.1.1 MR Optimization

In order to optimize the imaging parameters for diffusion acquisition, both T1 and T2 relaxation time of the brain tissue was measured in increasing concentrations of the gadolinium-based contrast agent. Omniscan rapidly reduced both T1 and T2 relaxation times in all regions of interest of native PND3 brains (Table 3, Table 4). The optimal concentration of Omniscan was found to be 0.5 mM, which sufficiently shortened T1 to enable reasonable acquisition times while leaving T2 values long enough to obtain both T2-weighted and diffusion-weighted scans (Figure 8).

Table 3. T1 relaxation times (ms) from the PND3 optimization series of C57/Bl6 animals. All samples were soaked in the listed concentration for 4 days prior to scanning.

Omniscan (mM)	cortex	striatum	hippocampus	ventricle
(PBS only)	1525.2	1459	1517.5	1348.1
0.25	633.5	602.2	586.6	574.6
0.5	466.7	437	422.1	413.8
1	291.9	236.4	277	310
5	53.75	53.15	53.3	53.2

Table 4. T2 relaxation times (ms) for the optimization series.

Omniscan (mM)	cortex	striatum	hippocampus	ventricle
(PBS only)	102.9	104.4	87.4	93
0.25	93.3	73.2	76.5	71.4
0.5	68.7	53.2	62.6	57.9
1	63.1	55	53.1	52.5
5	26.3	25.4	25.9	24.5

T1 and T2 maps were somewhat different for the study series CD1 strain animals (Table 5, Table 6) but not so significantly to warrant a change in the Omniscan concentration used. TR and TE values however were adjusted for each time point in the study.

Table 5. T1 relaxation times (ms) for representative brains from the study series.

Sample age	cortex	striatum	hippocampus	ventricle
PND3	204.7	214.7	227.9	209.0
PND7	190.0	192.8	179.5	185.0

Table 6. T2 relaxation times (ms) for representative brains from the study series.

Sample age	cortex	striatum	hippocampus	ventricle
PND3	61.0	57.4	60.6	53.0
PND7	50.8	49.4	56.7	49.3

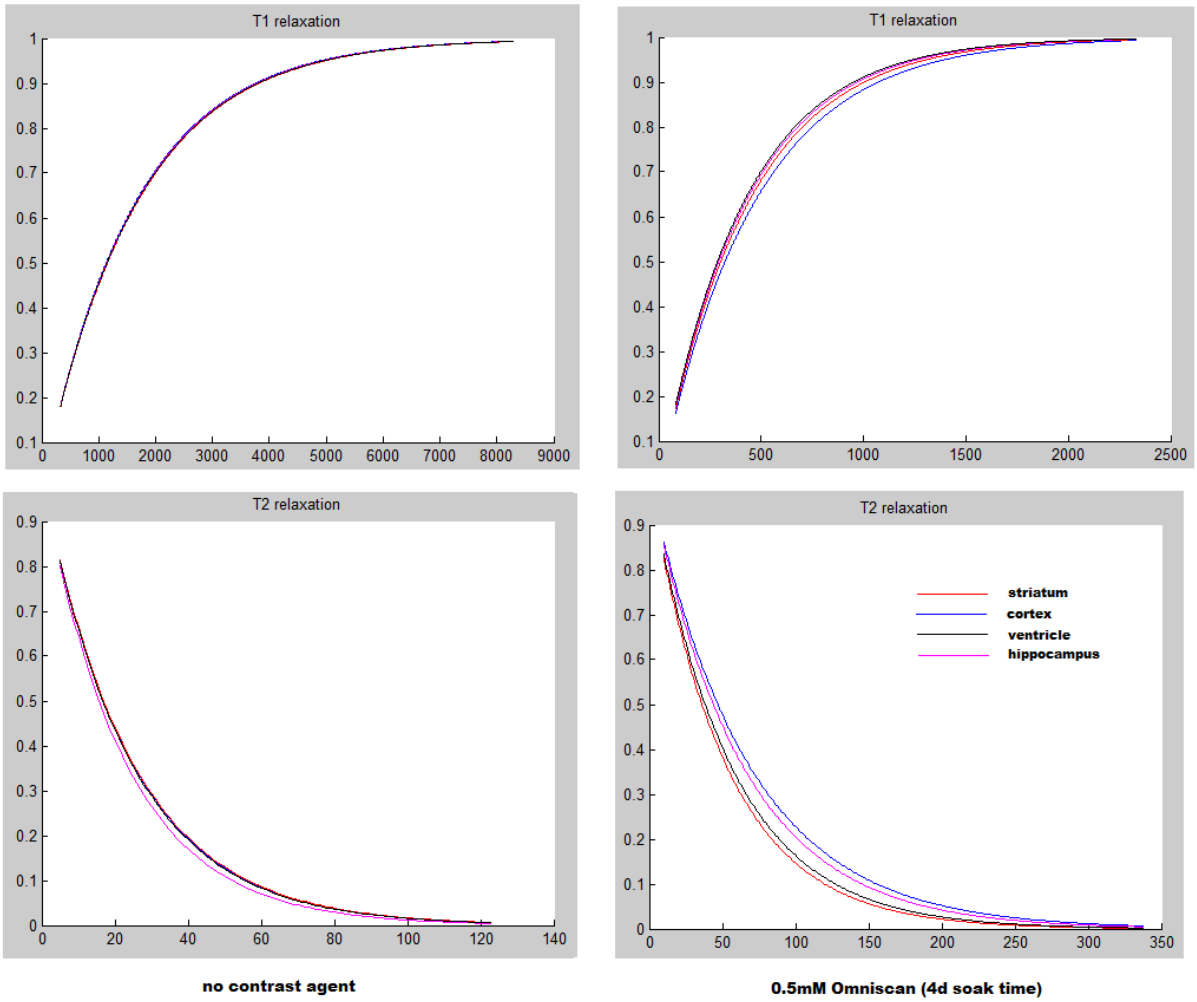

Figure 8. T1 and T2 relaxation curves for various tissues in a PND3 brain with either native contrast (left side) or with Omniscan, 0.5mM, the concentration ultimately used.

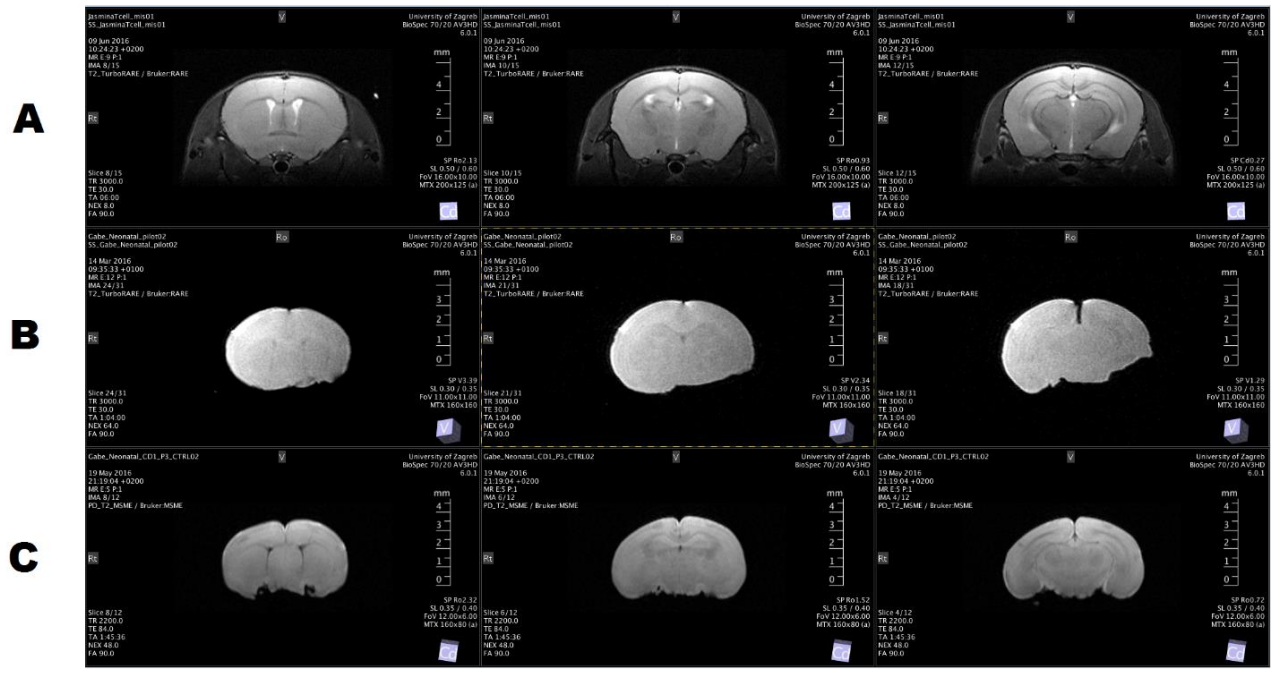

Figure 9. Representative T2-weighted images of coronal brain sections of an in vivo adult mice brain (A), native postnatal day 3 mice brain with TR and TE parameters unchanged from those used for row A (B) and postnatal day 3 mice brain immersed in 0.5 mM Omniscan for 4 days prior to scanning (C) with optimized TR and TE parameters.

6.1.2 MR Scans

In the sham operated animals DWI and T2WI data were normal in both hemispheres for both periods of observation, e. g. PND3 and PND7 (Figure 10 D, Figure 11 C, Figure 12 D, Figure 13 C). For the HI animal groups the T2WI hyperintensity was observed in the PND3 group in the occluded left MCA region, mainly involving the hippocampus, overlying cortex and partially the lateral caudoputamen (Figure 10 A, B). The T2WI hyperintensity seen on the PND3 group was drastically diminished in the PND7 group (Figure 12 A, B), but still a pronounced thinning of the corpus callosum could be observed. DWI hyperintensity was consistent with the T2WI observations for the PND3 animal group showing abnormal morphology of the hippocampus, overlying cortex and lateral caudoputamen (Figure 11 A, B). Interestingly morphological changes in the PND7 animal group mainly involved extreme thinning of the corpus callosum with visible alternations in the structure of the underlying hippocampus as seen with DWI (Figure 13 A; B)

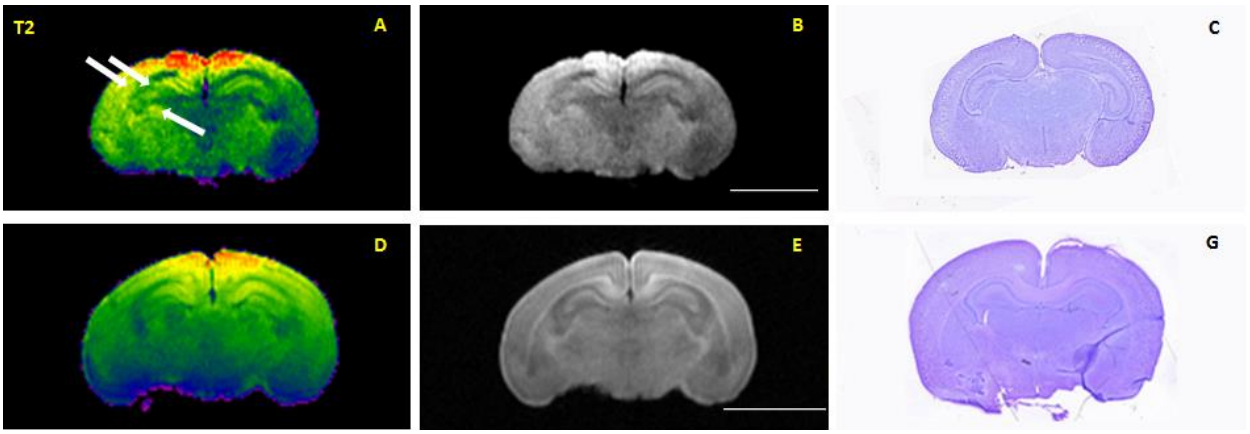

Figure 10. Comparison between corresponding coronal brain slices of the same brains obtained by T2-weighting MR imaging, presented in raw format (A, D), color enhanced visualization (B, E), and Nissl staining (C, G). The upper row of images presents visualization of coronal postnatal day 3 brain sections after hypoxic-ischemic injury **(**A, B, C**).** Arrows indicate hyperintensity on T2W images occurred in the cortex, hippocampus and thalamus of the ipsilateral hemisphere. The lower row of images presents sham-operated postnatal day 3 animals with no visible alternations in brain morphology between the two hemispheres **(**A, C, E). Bars: 5mm.

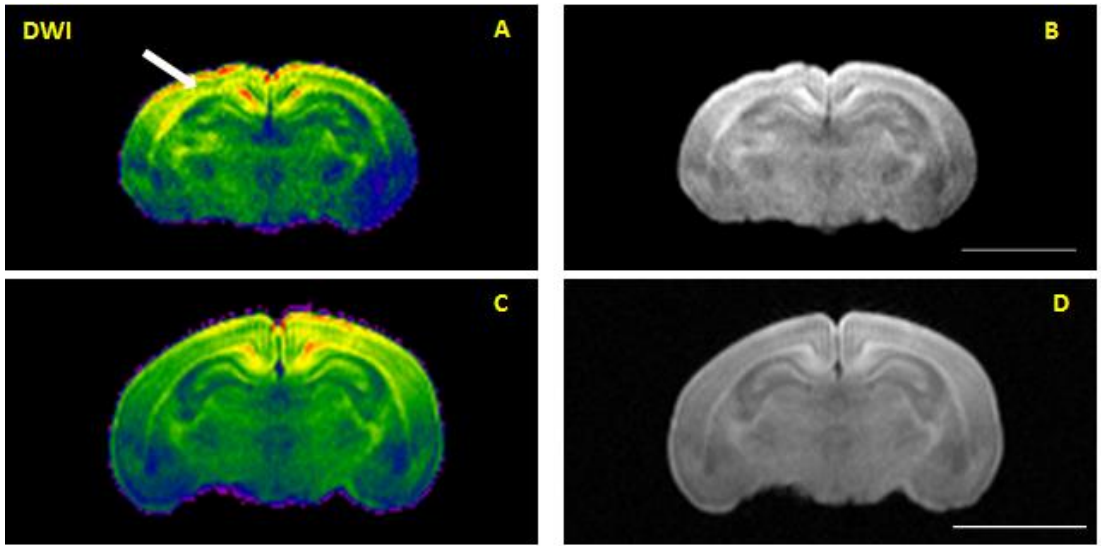

Figure 11. Representative diffusion weighted images of coronal postnatal day 7 brain sections after hypoxic-ischemic injury presented in raw format (A**;** color enhanced (B) compared to sham-operated controls (C; color enhanced D). Arrow indicates pronounced thinning of the hippocampus of the ipsilateral hemisphere (A) compared to no visible morphological change in the structure of the control sham-operated brain. Bars: 5mm.

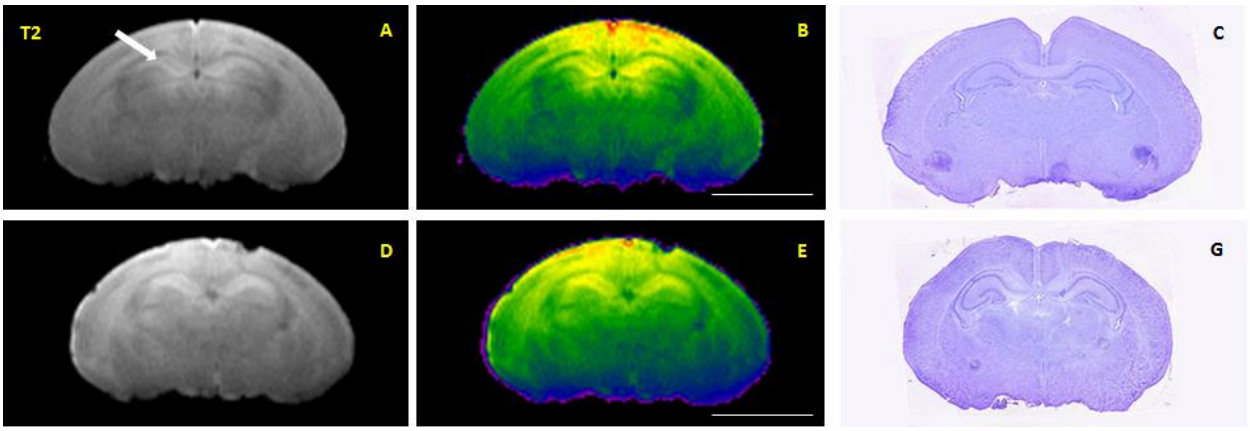

Figure 12. Comparison between corresponding coronal brain slices of the same brains obtained by T2-weighting, presented in raw format (A, D), color enhanced visualization (B, E), and Nissl staining (C, G). The upper row of images presents visualization of coronal postnatal day 7 brain sections after hypoxic-ischemic injury (A, B, C). Arrow indicates changes in the corpus callosum and underlying hippocampus of the ipsilateral hemisphere. The lower row of images presents sham-operated postnatal day 7 animals with no visible alternations in brain morphology between the two hemispheres (A, C, E). Bars: 5mm.

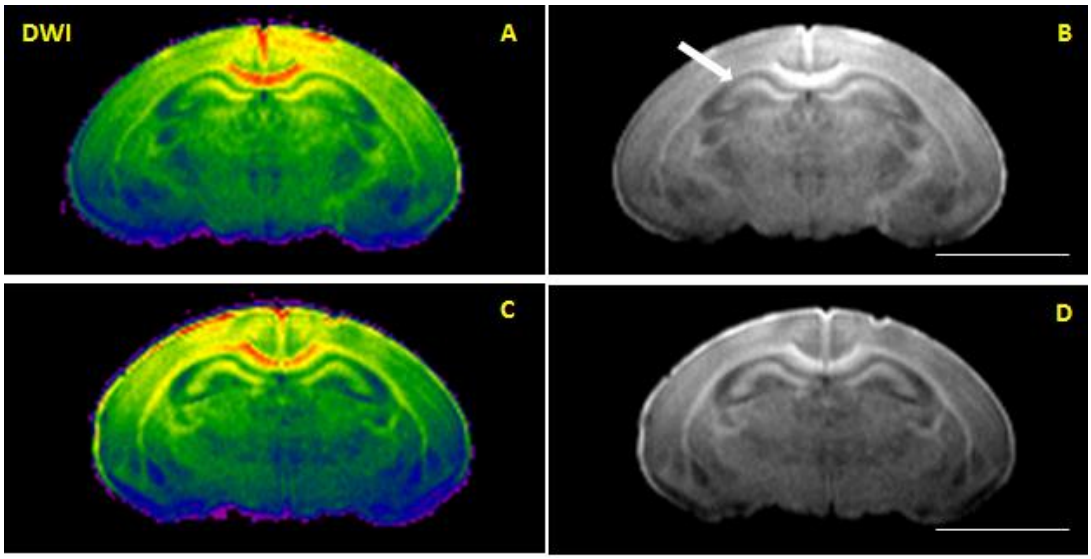

Figure 13. Representative diffusion weighted images of coronal postnatal day 7 brain sections after hypoxic-ischemic injury presented in raw format (A**;** color enhanced (B) compared to sham-operated controls (C; color enhanced D). Arrow indicates pronounced thinning of the hippocampus of the ipsilateral hemisphere (A) compared to no visible morphological change in the structure of the control sham-operated brain. Bars: 5mm.

6.2 Histopathological examination of brain tissue

In order to validate the extent of the pathohistological changes occurring after inducing HI in PND0 mice, Nissl stained histological sections from animals sacrificed at PND3 and PND7 were inspected. Neuronal cells in the cortex, hippocampus and striatum of both PND3 (Figure 14) and PND7 (Figure 16) showed no evident neuronal damage for the sham-surgery group. Hippocampal cells appeared normal and were arranged in neat rows, and were large and round for control PDN3 animals (Figure 14, 1, 2, 3, 4, 8, 9, 10, 11) as well as control PDN7 animals (Figure 16, 1, 2, 3, 4, 8, 9, 10, 11). The morphology of the layers of the cells of the cortex (Figure 14-5 for PND3; Figure 16-12 for PND7) and striatum (Figure 14-6,7 for PND3; Figure 16-13,14 for PND7) were clear and complete with clearly visible nucleoli. Nissl bodies were equidistributed around the nucleus, with rules and without cavitation.

The pathological alterations were prominent in the left hemisphere (ischemic) of both PND3 and PND7 HI groups, characterized by a large number of pyknotic nuclei and/or edematous cells compared to the control sham-operated group but also compared to the contralateral side (Figure 15 ipsi and contra, Figure 17 ipsi and contra).

In the PND3 isolated group of animals, aberrant morphology was visible after inducing HI in the hippocampus (Figure 15-1, 2, 3, 4, 6, 7) and striatum (Figure 15-6, 7) of the left ischemic hemisphere compared to the contralateral hemisphere (Figure 15-8, 9, 10, 11, 13, 14) and control sham-operated group (Figure 14). Cells of the striatum were clearly triangular in shape mostly exhibiting a dark staining due to condensation of cytoplasm and karyoplasm surrounded by clear edematous tissue. The Nissl bodies were blurred or absent, with vacuolization, a disordered arrangement and formation of a network. The morphology of pyramidal cells changed significantly compared with the sham-surgery group. Morphological features included a disordered arrangement of the cells, significant loss in volume especially visible as thinning of the stratum oriens in the CA1 and CA2 regions. There was even apparent cell death and cell loss, and the normal pyramidal cells were scattered within the background of the dead cells. Slightly visible alternations were seen in the cortex of the ischemic hemisphere as disordered arrangement of the cells with features of edema.

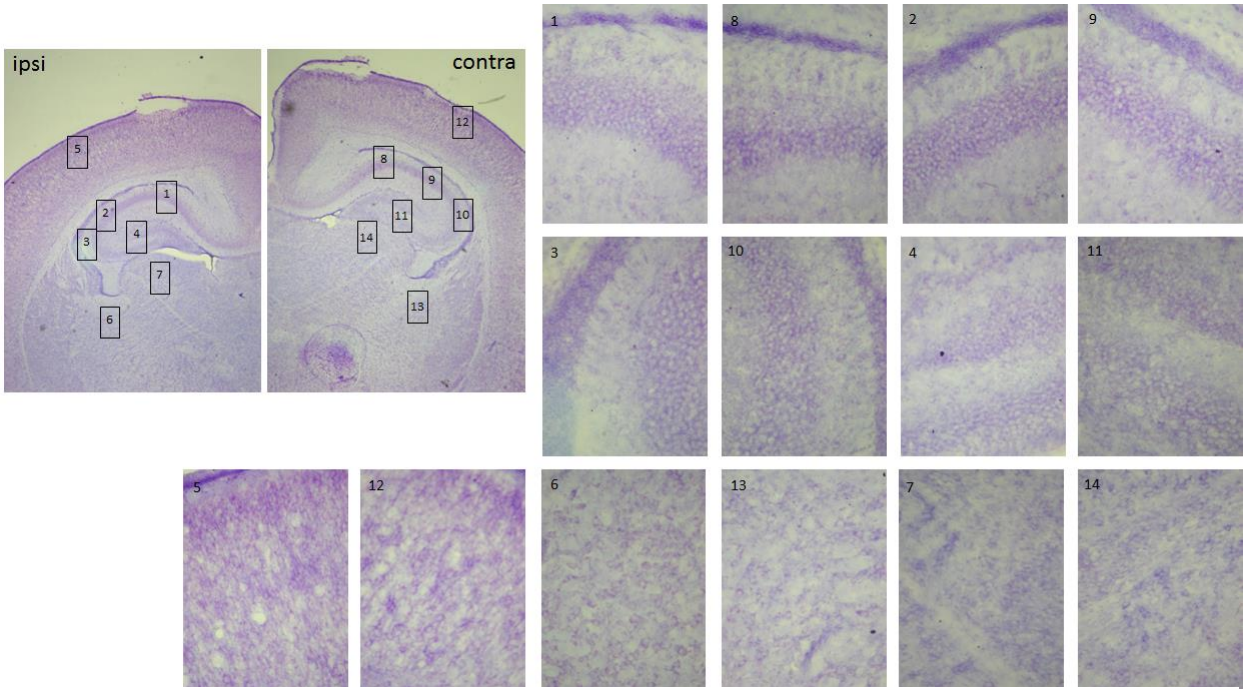

Figure 14. Animal 2-2 Representative histological sections of Nissl staining of brains of postnatal day 3 sham-operated mice. On the left upper side 10x magnification of the healthy left hemisphere (ipsi) and next to it healthy right (contra) hemisphere. Nissl staining of neurons in the CA1 (1), CA2 (2), CA3 (3), dentate gyrus (4), cortex (5), fimbria (6) and thalamus (7) of the left hemisphere show no showed no evident neuronal damage. No apparent neuronal damage is seen in the CA1 (8), CA2 (9), CA3 (10), dentate gyrus (11), cortex (12), fimbria (13) and thalamus (14) of the right contralateral hemisphere. Barr: 20 μm.

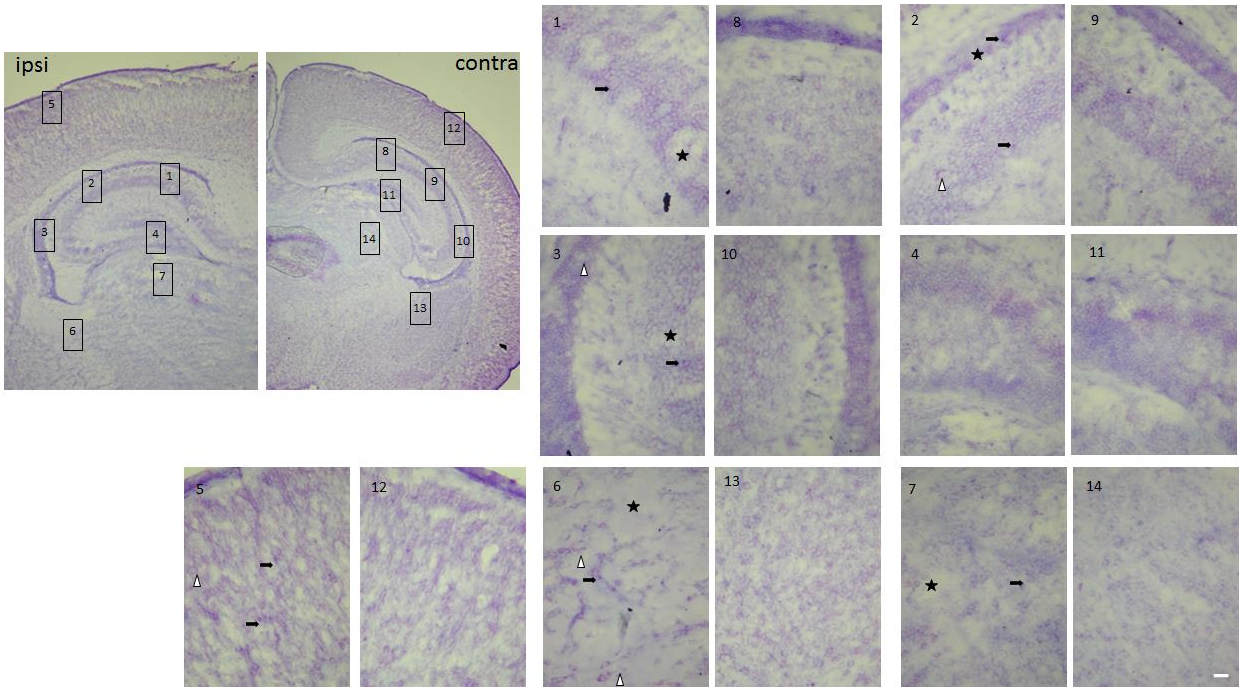

Figure 15. Animal 2-6 Representative histological sections of Nissl staining of brains of postnatal day 3 mice 3 days after hypoxia-ischemia. On the left upper side 10x magnification of the left ipsilateral hemisphere (ipsi) and next to it right contralateral hemisphere (contra). Nissl staining of neurons in the CA1 (1), CA2 (2), CA3 (3), dentate gyrus (4), cortex (5), fimbria (6) and thalamus (7) of the left hemisphere show prominent pathological alterations characterized by a large number of pyknotic (arrow) and edemtous (triangle) cells sourounded by clear edematous tissue (star). No apparent neuronal damage is seen in the CA1 (8), CA2 (9), CA3 (10), dentate gyrus (11), cortex (12), fimbria (13) and thalamus (14) of the right contralateral hemisphere. Barr: 20 μm.

The pathological alterations were even more prominent in the ipsilateral hemisphere in the PND7 animals of the HI group compared to the contralateral hemisphere (Figure 17-ipsi and contra) or the sham operated group (Figure 16). At 7 days following HI signs of tissue edema disappeared but a significant loss of volume especially visible as thinning or absence of the stratum oriens of the CA1 and CA2 (Figure 17-1, 2) and a prominent thinning of the corpus callosum (Figure 17–ipsi). A notable number of cells in the striatum and cortex were clearly triangular in shape mostly exhibiting a dark staining due to condensation of cytoplasm and karyoplasm but with less prominent cell loss than that seen in PND3 animals (Figure 17-5, 6).

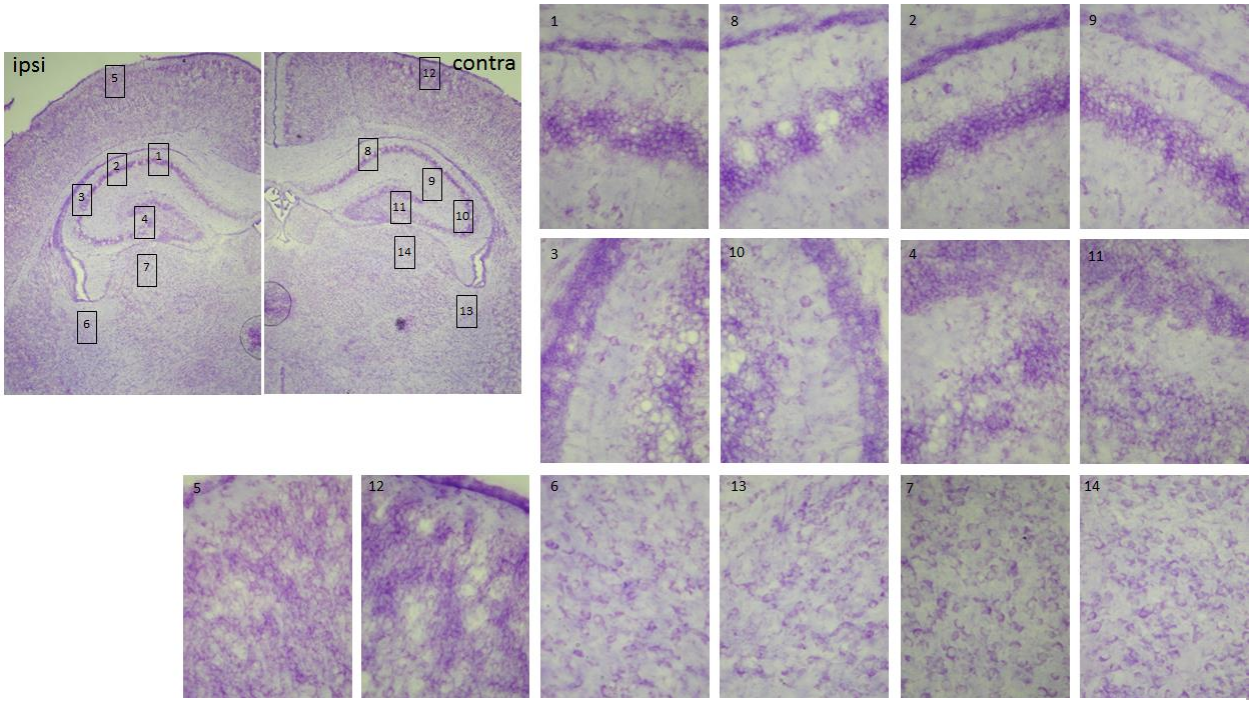

Figure 16. Animal 2-15 Representative histological sections of Nissl staining of brains of postnatal day 7 sham-operated mice. On the left upper side 10x magnification of the healthy left hemisphere (ipsi) and healthy right (contra) hemisphere. Nissl staining of neurons in the CA1 (1), CA2 (2), CA3 (3), dentate gyrus (4), cortex (5), fimbria (6) and thalamus (7) of the left hemisphere show no showed no evident neuronal damage. No apparent neuronal damage is seen in the CA1 (8), CA2 (9), CA3 (10), dentate gyrus (11), cortex (12), fimbria (13) and thalamus (14) of the right contralateral hemisphere. Barr: 20 μm.

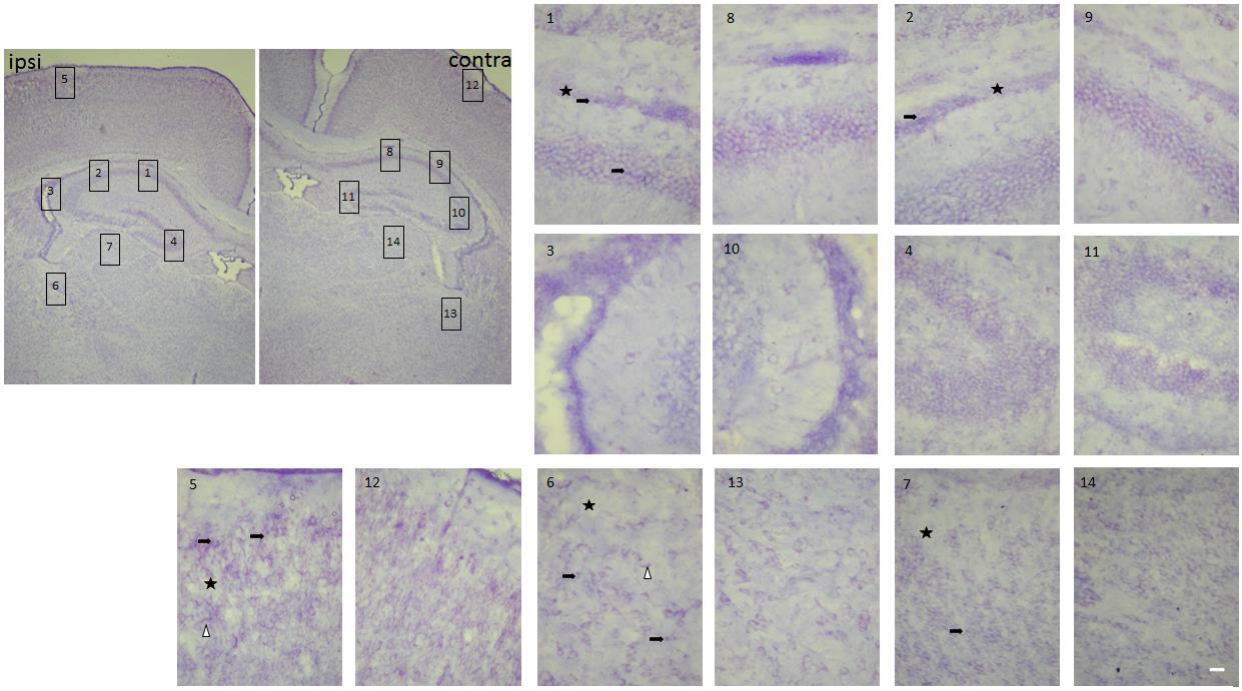

Figure 17. Animal 2-10 Representative histological sections of Nissl staining of brains of postnatal day 7 mice 7 days after hypoxia-ischemia. On the left upper side 10x magnification of the left ipsilateral hemisphere (ipsi) and next to it right contralateral hemisphere (contra). Nissl staining of neurons in the CA1 (1), CA2 (2), CA3 (3), dentate gyrus (4), cortex (5), fimbria (6) and thalamus (7) of the left hemisphere show prominent pathological alterations characterized by a large number of pyknotic (arrow) and edematous (triangle) cells sourounded less edematous tissue (star). No apparent neuronal damage is seen in the CA1 (8), CA2 (9), CA3 (10), dentate gyrus (11), cortex (12), fimbria (13) and thalamus (14) of the right contralateral hemisphere. Barr: 20 μm.

6.3 Immunohistochemistry

Apoptotic cells can be found in the HI injured hemisphere. In order to detect apoptotic cells in the brain of PND3 and PND7 mice after HI injury we performed analysis of cleaved Caspase-3 stained sections performed on 25 μm sections adjacent to the Nissl-stained sections (Figure 18). Caspase-3-immunoreactive protein was expressed in PND3 mice in injured cortical regions (Figure 18A), striatum, hippocampus (Figure 18B), and thalamus, regions shown previously to be selectively vulnerable to hypoxic ischemic injury in newborn rodents. Some of the cleaved Caspase-3 cells were also positive for neuronal nuclei NeuN staining confirming presence of neuronal apoptosis in this model of HI. The cerebral cortex in normal control brains and in hemispheres contralateral to the ligation showed only sparse caspase-3

immunoreactivity. Clear caspase-3 immunoreactivity was not found in PND7 animals with HI injury or in sham-operated controls (Figure 18C).

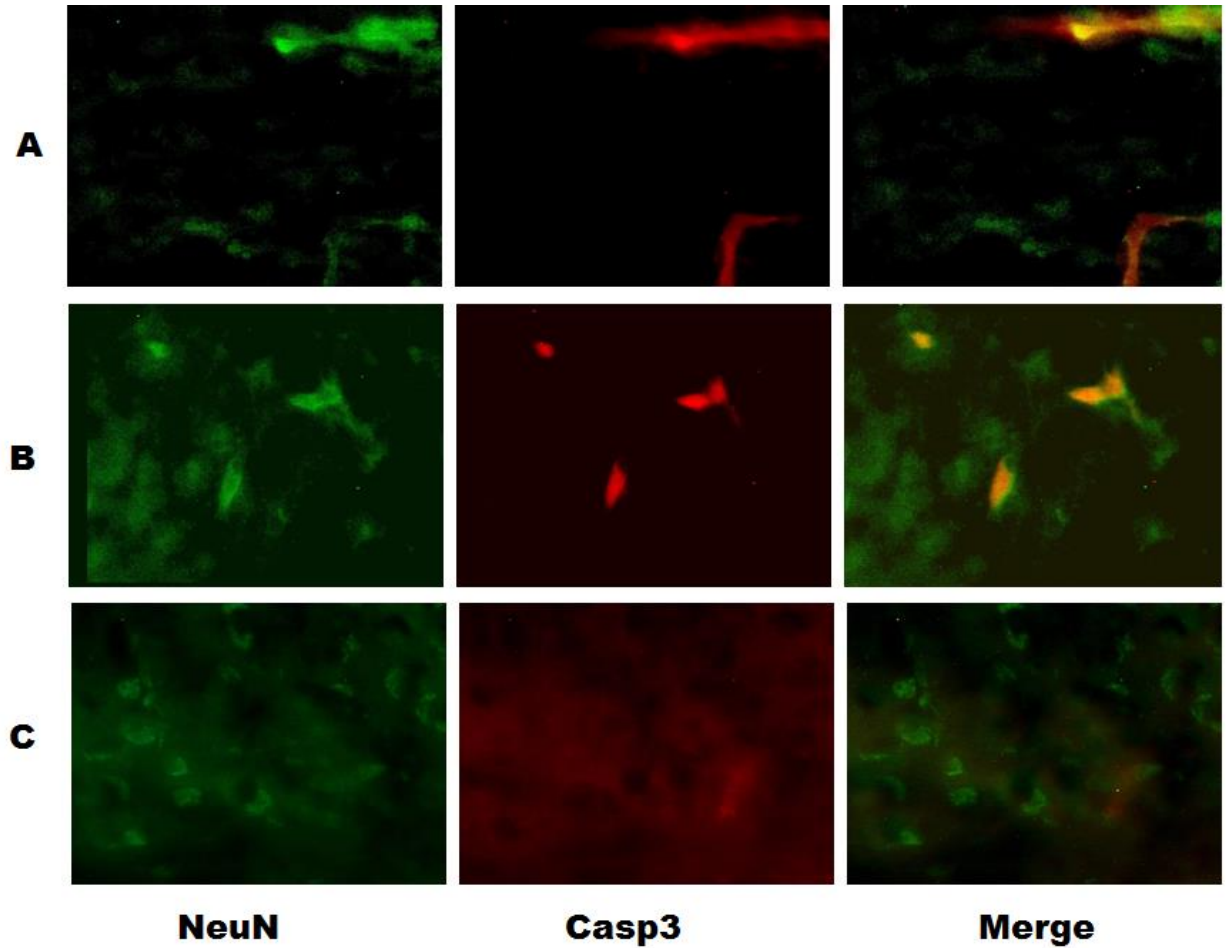

Figure 18. Neuronal nuclei and caspase-3 immunostaining 72 hours after hypoxic-ischemic injury (HI). Representative fluorescent High-magnification images from 25 µm sections sections of cortex (A), and the CA1 region of the hippocampus (B) on the ligated side showing apoptotic cells stained with anti-cleaved Caspase-3 antibody. Noninjured areas, in right contralateral hemisphere with only nonparticulate background staining (C). Scale bar: 10 µm.

6.4 Sex Determination via Genotyping

Since male sex is a well-established risk factor for poor neurodevelopmental outcome following premature birth and the mechanisms behind this sex-related difference are unknown

we followed determination of sex by genotyping since PND3 and PND7 animals were too young to be easily sexed by visual inspection (Figure 19).

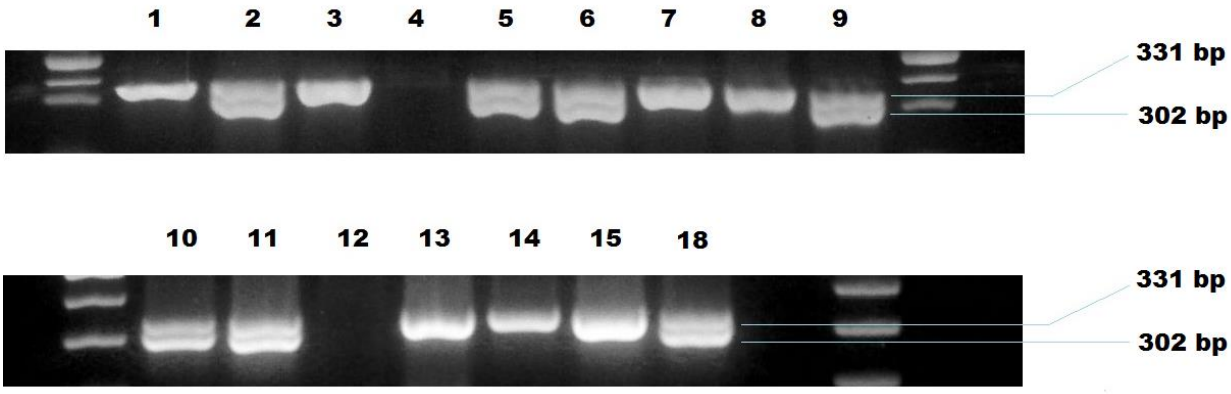

Figure 19. Gel electrophoresis of the PCR products following amplification with gender-genotyping primers. Column numbers correspond to animal numbers listed in Table 1. Female sex is represented with a band at 331 bp, while male sex is represented with both 302 bp and 331 bp bands.

7 DISCUSSION

The main objective of this thesis was to establish a mice hypoxic-ischemic brain injury model in the postnatal day 0 neonatal mouse along with developing new methods for ex vivo MR imaging of neonatal hypoxic ischemic brain injury to enable evaluation of tissue damage and injury progression. A veritable menagerie of neonatal species such as rats, mice, rabbits, sheep, pigs or monkeys have been used to produce study brain damage induced by HI at different stages of brain development (Rumajogee et al. 2016). These animal models have provided the basis for depicting the physiological and biochemical mechanisms of brain injury. Among HI models, the fetal and newborn rhesus monkey have been used and due to physiological and neuroanatomical similarities to humans (Adamsons et al. 1963). In contradistinction to primates, advantages accruing to rodents include easy and fast breeding, short pregnancy, large litters, and low maintenance costs. The postnatal day 7 rat was originally chosen for study as at this stage of development because its brain is histologically similar to that of a 32- to 34-week gestation human fetus or newborn infant with the specific features which include completion of cerebral cortical layering, presence of myelinated white

matter and involution of germinal matrix, with specific immune inflammatory changes (Jiang et al. 1999, Clancy et al. 2001, Vannucci 1993). However, there are numerous drawbacks in the original RV method. First, the usage of halothane during anesthesia can inhibit the respiration and circulation. Also in the original report the left CCA was merely ligated, creating the ambiguity that subsequent recanalization may confound findings at later time points.

Therefore minor modification of the Rice-Vanucci method were performed as described previously. In the present study, the anesthesia isoflurane was selected instead of halothane which provided short induction, good muscle relaxation, with no inhibition of the circulation or respiration. Then in the present study we performed a double ligation of the CCA after isolation and cut between the ligatures, to avoid the formation of blood reperfusion (Nakajima, et al. 2000). Accuracy of unilateral carotid artery ligation is fundamental, and there is a great need of right identification of the arterial pulse prior to making a permanent ligation and cut, in order to avoid mistaking the neck muscles for vascular. Also the ambient temperature in the chamber should be maintained at 37±0.5°C in order to avoid temperature changes which can affect the mortality rate. Also, hypothermia has been shown to have a protective effect on HI; indeed as mentioned previously therapeutic hypothermia is currently the standard of care for term newborns suffering hypoxic insults. Therefore, it is crucial to control the temperature with a water bath to ensure the modeling effort as even a few degrees of cooling has been found to confer protective effects (Wood et al. 2016).

The extension of the RV model to PND0 mice offers potential advantages relative to RV studies in PND1 rats which have been previously described (Sheldon et al. 1996, McQuillan et al. 2003). The technical challenge of performing surgery on very small animals proved surmountable with dedication and practice. Once proficiency was reached very low intraoperative losses (<5%) were achieved, and a procedure time of 5-7 minutes per animal was typical. Perhaps the single most important motivation for the use of mice is the ready availability of transgenic strains, some of which have already been studied using the RV model albeit in older neonates (Pimentel-Coehlo et al. 2013, Scafidi et al. 2014). Beyond these factors, mice offer a considerable cost savings relative to rats, however, rats do allow for a richer and generally more clinically relevant battery of behavioral comparisons. Finally,

since it has been shown that even differences in strain can have a very significant effect on the course of HI pathology (Sheldon et al. 1998), species differences surely exist as well. Therefore it is worthwhile to discover the physiology of PND0 mice in the context of HI.

Beyond species-specific interests, the resistance of fetal and newborn animals to HI generally, relative to their older counterparts, is in itself an active area of inquiry. In our pilot studies it was observed that PND0 animals could withstand 3 to 4 times the duration of hypoxia as PND7 pups, in agreement with previous reports. The physiological factors underlying this comparative robustness are multifactorial and not fully understood (Perlman 2007). Hence while PND7 rats and mice may approximate the neurodevelopmental stage of term infants, HI studies in such animals may not engage resistance mechanisms that are ephemeral to the interpartum phase, thus controlled HI studies of hours-old animals such as the one presently described may inform this crucial period.

Light microscopy analysis showed cellular swelling and degeneration, nuclear condensation and fragmentation, the Nissl body was blurred or absent, cytoplasm was vacuolated and the endoplasmic reticulum was deranged. Morphological alterations were more prominent in the neurons of the cerebral cortex and hippocampus in the hemispheres ipsilateral to CCA ligation, demonstrating the effectiveness of the procedure. Edematous cells and cells with pyknotic nuclei were apparent in the ipsilateral side but absent contralaterally. There was a visible thinning of the stratum oriens in the ipsilateral CA1 and CA2 hippocampal regions, an effect which was noticeable in PND3 HI specimens and became more pronounced by PND7. Subtle disorder and edema was appreciable in the ipsilateral cortex of HI animals. The ipsilateral cortex and CA1 hippocampal region was also found to be populated with cells doubly labeled for cleaved caspase 3 and NeuN, which were absent from the contralateral side in HI animals as well as sham-operated controls. While the PCR method successfully determined the gender of the study animals, greater numbers will be required in future studies to detect any gender-specific effects. Together, these data confirm the successful implementation of the RV model in this series, establishing a foundation for follow-up investigations.

The average adult human brain is around 3000 times bigger than an average adult mouse brain (Badea et al. 2009). In order to delineate morphological features of the mouse

brain, a spatial resolution of 0.1 mm is often needed, to compensate for the reduction in voxel size and proportionally the decrease in signal originating from it. The reduction in signal can be compensated by using high field magnets (7T or higher), high-sensitivity coils, using contrast agents and more signal averages, at the expense of prolonged acquisition time. Using post-mortem ex vivo imaging fits these conditions, providing greater spatial resolution due to the lack of imaging time constraints and movement artifacts and offering the opportunity to use tighter fitting coils, providing higher SNR (Lerch et al. 2012). However, post-mortem studies rely on specimen fixation to inhibit tissue decay which unfortunately substantially alters tissue diffusivity profiles. T_1 and T_2-weighted and diffusion-weighted MRI have been commonly used to study the developing mouse brain (Mori et al. 2006, Petiet et al 2008, Zhang et al. 2012). However, due to a lack of naïve early white matter tracts contrast, application of Gadolinium (Gd)-based contrast agents in useful to increase signal-to-noise ratio (SNR). Previous studies showed that contrast agents can penetrate the tissue specimens via unknown mechanisms, and significantly shorten the $T_1$and T_2 relaxation times of mouse brain tissue, enhancing signals and tissue contrasts (Sharief et al. 2006, Cleary 2011). In MR imaging, the signal from any tissue is dependent on the water content of the tissue and how it is bound. By choosing different acquisition parameters and contrast agent compounds and concentrations, physical interactions of the water protons with the tissue can be altered to optimize tissue contrast. As seen in Figure 8, the T1 signal is dependent primarily on differential recovery, of the distinct tissue types, of signal between the individual radiofrequency pulses used to stimulate the tissue; in this scenario the differential was insufficient, even with contrast agent added, to produce a good SNR. On the other hand, T2 contrast in Figure 8, dependent on the differential spin spin relaxation time between tissues (Sharief et al. 2006), improved with incubation in Gd-based contrast agent, increasing the SNR of the ex vivo brains.

Comparing diffusion-weighted and T2-weighted MR imaging to Nissl staining for visualization of the injured area we showed correlative distribution of pathological damage. In vivo studies have reported good correlation between the areas of increased signal intensity on DWI and T2WI and histological distribution of pathological damage from 24 to 72 hours after HI (Meng et al. 2004, Tuor et al. 1998, Qiao et al. 2002). The hyperintensity detected on T2WI is generally interpreted as indication of vasogenic edema or lesion formation which

persists in the first 24 to 72 hours after HI (Tuor et al. 1998, Rumpel et al. 1997). This is consistent with our finding showing T2WI hyperintensity in the group of animals isolated 72 hours after HI which comprised the region perfused middle cerebral artery flow, e.g. the hippocampus, overlying cortex and part of the lateral caudoputamen. The observed T2WI hyperintensity seen on the postnatal day 3 group was not detectable one week after HI evidencing the resolution of the vasogenic edema after HI. Both findings on PND3 and PND7 animals were consistent with hisological Nissl stained brains on which pathological alterations were prominent in the left hemisphere as patches of clear edematous tissue in the CA1 and CA2 areas of the hippocampus, cortex and thalamus in the PND3 animal group, resolving by PND7, 7 days after HI.

Our results demonstrate that the use of DWI in for the first 72 hours after HI in ex vivo neonatal brains is much less sensitive than T2WI which changes with time giving more SNR thus better visualization of the morphology after 7 days. Increased diffusion-weighted imaging signal after severe ischemia is thought to be at least in part due to cytotoxic edema (Moseley et al. 1990). Since water in the extracellular space shows more random water diffusion than that in the intracellular space, these changes in water balance should result in a decrease of tissue diffusion. Diffusion-weighted imaging can detect this decrease in water diffusion, which is shown as an area of increased signal. In vivo human studies show that sensitivity of diffusion-weighted imaging to adult cerebral infarction is up 99% (van Everdingen et al. 1998, Lovblad et al. 1998), but are less sensitive for neonatal HI--around 50%--which is explained mainly by differences between the water content of the neonatal and adult brain. The neonatal brain has a much higher water content than the adult brain, and correspondingly lower fat content, which is minimal until PND7, not increasing to adult levels until approximately P23 (Foran 1992). Therefore the neonatal brain features increased water diffusion such that decreased water diffusion after ischemia is less discernible than in adult brains (Neil et al. 1998). Additionally, perfusion and fixation alternates the brain structure by crosslinking the proteins thus altering the water diffusivity further decreasing sensitivity to pathology detection (Sun et al. 2005).

8 CONCLUSION

Herein we have presented MR images of ex vivo brains as well as histological and immunohistochemical evidence detailing the effect of HI created within the RV framework on PND0 mice for the first time. These data illustrate the functionality of the model and give a basis for further work. Future studies are contemplated, including a focus on the effect on oligodendrocytes, gliosis, necrotic as well as apoptotic neurons, studies involving later time points, larger numbers of specimens, behavioral investigations, in vivo imaging and comparison of strain differences.

Additionally we have developed a relatively high throughput MRI scanning protocol suitable for scanning several specimens in reasonable time period, with a scan quality sufficient to identify pathology which was subsequently verified by sectioning and staining of the imaged samples.

To some degree all models of perinatal HI suffer from inter-animal variability, including the RV model, the current instantiation being no exception. However the strength of the RV model is that it invokes hemispheric pathology, allowing the contralateral side to serve as an effective control (though true sham operated controls are vital to verify the validity of this practice) allowing more significant comparisons to be asserted. By extending this popular paradigm to PND0 mice, and incremental but significant expansion of its applicability has been achieved.

9 ACKNOWLEDGEMENTS

The author would like to thank Marina Dobrivojević, Lada Brkić, Siniša Škokić, Srećko Gajović, Dinko Mitrečić, Sandra Grgić, Dunja Gorup, Ivan Alić, Olja Ulični, Roland Pochet, Marija Renić, Aleksandra Šindić, Dora Polsek and Caroline Borden for all their support and tutelage. Special recognition is due to Siniša Škokić for performing the MR scans contained herein, and to Sandra Grgić, who performed the genotyping of the animals. Thanks also to Matthias Hoehn of the In Vivo NMR Research Group at the Max Planck Institute for Metabolism Research, Cologne, Germany, where the initial MR optimization studies were conducted. This study was supported by EU FP7 grant GlowBrain (REGPOT–2012–CT2012–316120)

10 REFERENCES

1. Adamsons K, Behrman R, Dawes GS, Dawkins MJR, James LS, Ross BB. The treatment of acidosis with alkali and glucose during asphyxia in foetal rhesus monkeys. The Journal of physiology. 1963;169(3):679–689.

2. Aden U, Dahlberg V, Fredholm BB, Lai L-J, Chen Z, Bjelke B. MRI Evaluation and Functional Assessment of Brain Injury After Hypoxic Ischemia in Neonatal Mice. Stroke. 2002 May 1;33(5):1405–10.

3. Aggarwal M, Burnsed J, Martin LJ, Northington FJ, Zhang J. Imaging neurodegeneration in the mouse hippocampus after neonatal hypoxia-ischemia using oscillating gradient diffusion MRI: MRI in a Mouse Model of Neonatal HI. Magnetic Resonance in Medicine. 2014 Sep;72(3):829–40.

4. Alexander M, Garbus H, Smith AL, Rosenkrantz TS, Fitch RH. Behavioral and histological outcomes following neonatal HI injury in a preterm (P3) and term (P7) rodent model. Behavioural Brain Research. 2014 Feb;259:85–96.

5. Anderson R, Maga AM. A Novel Procedure for Rapid Imaging of Adult Mouse Brains with MicroCT Using Iodine-Based Contrast. PloS one. 2015;10(11):e0142974.

6. Arin-Padilla M. Developmental Neuropathology and Impact of Perinatal Brain Damage. II. Journal of Neuropathology and Experimental Neurology. 1997;56(3):219-235.

7. Ashwini CA, Shubha R, Jayanthi KS. Comparative anatomy of the circle of Willis in man, cow, sheep, goat, and pig. Neuroanatomy. 2008;7:54–65.

8. Back SA, Luo NL, Borenstein NS, Levine JM, Volpe JJ, Kinney HC. Late oligodendrocyte progenitors coincide with the developmental window of vulnerability for human perinatal white matter injury. The Journal of Neuroscience. 2001;21(4):1302–1312.

9. Back SA, Miller SP. Brain injury in premature neonates: A primary cerebral dysmaturation disorder?: Premature Cerebral Dysmaturation. Annals of Neurology. 2014 Apr;75(4):469–86.

10. Badawi N, Kurinczuk JJ, Keogh JM, Alessandri LM, O'Sullivan F, Burton PR, et al. Antepartum risk factors for newborn encephalopathy: the Western Australian case-control study. Bmj. 1998;317(7172):1549–1553.

11. Badea A, Johnson GA, Williams RW. Genetic dissection of the mouse CNS using magnetic resonance microscopy: Current Opinion in Neurology. 2009 Aug;22(4):379–86.

12. Behrman RE, Butler AS, Institute of Medicine (U.S.), Committee on Understanding Premature Birth and Assuring Healthy Outcomes. Preterm birth: causes, consequences, and prevention [Internet]. Washington, D.C.: National Academies Press; 2007 [cited 2016 Jun 27].

13. Bergmann O, Bhardwaj RD, Bernard S, Zdunek S, Barnabe-Heider F, Walsh S, et al. Evidence for Cardiomyocyte Renewal in Humans. Science. 2009 Apr 3;324(5923):98–102.

14. Bryant DM, O'Meara CC, Ho NN, Gannon J, Cai L, Lee RT. A systematic analysis of neonatal mouse heart regeneration after apical resection. Journal of Molecular and Cellular Cardiology. 2015 Feb;79:315–8.

15. Buser JR, Maire J, Riddle A, Gong X, Nguyen T, Nelson K, et al. Arrested preoligodendrocyte maturation contributes to myelination failure in premature infants. Annals of Neurology. 2012 Jan;71(1):93–109.

16. Busl KM, Greer DM. Hypoxic-ischemic brain injury: pathophysiology, neuropathology and mechanisms. NeuroRehabilitation. 2010;26(1):5–13.

17. Calamante F, Tournier J-D, Kurniawan ND, Yang Z, Gyengesi E, Galloway GJ, et al. Super-resolution track-density imaging studies of mouse brain: Comparison to histology. NeuroImage. 2012 Jan;59(1):286–96.

18. Chandra S, Spitzer AR. Long-term effects of indomethacin prohylaxis in extremely-low-birth-weight infants. Clinical Pediatrics. 2002;41(3):190.

19. Chen H, Burris M, Fajilan A, Spagnoli F, Zhang JH, Tang J. Prolonged Exposure to Isoflurane Ameliorates Infarction Severity in the Rat Pup Model of Neonatal Hypoxia-Ischemia. Translational Stroke Research. 2011 Sep;2(3):382–90.

20. Chernoff EAG, Stocum DL, Nye HLD, Cameron JA. Urodele spinal cord regeneration and related processes. Developmental Dynamics. 2003 Feb;226(2):295–307.

21. Clancy B, Darlington RB, Finlay BL. Translating developmental time across mammalian species. Neuroscience. 2001;105(1):7–17.

22. Clancy B, Finlay BL, Darlington RB, Anand KJS. Extrapolating brain development from experimental species to humans. NeuroToxicology. 2007 Sep;28(5):931–7.

23. Clapcote S Roder J. Simplex PCR assay for sex determination in mice. BioTechniques. 2005;38(5):702-706.

24. Cleary JO, Wiseman FK, Norris FC, Price AN, Choy M, Tybulewicz VLJ, et al. Structural correlates of active-staining following magnetic resonance microscopy in the mouse brain. NeuroImage. 2011 Jun;56(3):974–83.

25. Craig A, Luo NL, Beardsley DJ, Wingate-Pearse N, Walker DW, Hohimer AR, et al. Quantitative analysis of perinatal rodent oligodendrocyte lineage progression and its correlation with human. Experimental neurology. 2003;181(2):231–240.

26. Dai X, Lercher LD, Clinton PM, Du Y, Livingston DL, Vieira C, et al. The trophic role of oligodendrocytes in the basal forebrain. The Journal of neuroscience. 2003;23(13):5846–5853.

27. Dean JM, Moravec MD, Grafe M, Abend N, Ren J, Gong X, et al. Strain-Specific Differences in Perinatal Rodent Oligodendrocyte Lineage Progression and Its Correlation with Human. Developmental Neuroscience. 2011;33(3–4):251–60.

28. Du Y, Dreyfus CF. Oligodendrocytes as providers of growth factors. Journal of Neuroscience Research. 2002 Jun 15;68(6):647–54.

29. Dunn PM. Dr William Little (1810-1894) of London and cerebral palsy. Archives of Disease in Childhood-Fetal and Neonatal Edition. 1995;72(3):F209–F210.

30. Feng Y, Lu S, Wang J, Kumar P, Zhang L, Bhatt AJ. Dexamethasone-induced neuroprotection in hypoxic-ischemic brain injury in newborn rats is partly mediated via Akt activation. Brain Research. 2014 Nov;1589:68–77.

31. Fitzgerald L. The oxygen consumption of neonatal mice. J Exp Zool. 1953;124(3):415-425.

32. Hammelrath L, Škokić S, Khmelinskii A, Hess A, van der Knaap N, Staring M, et al. Morphological maturation of the mouse brain: An in vivo MRI and histology investigation. NeuroImage. 2016 Jan;125:144–52.

33. Haubner BJ, Adamowicz-Brice M, Khadayate S, Tiefenthaler V, Metzler B, Aitman T, et al. Complete cardiac regeneration in a mouse model of myocardial infarction. Aging. 2012;4(12):966–977.

34. Husseini K, Huon C, Mokhtari M, Iniguez JL, Texereau J, Roche R, et al. 178 Pulmonary Function at one Year of Age in Premature Infants with Bronchopulmonary Dysplasia. Pediatric Research. 2005;58(2):385–385.

35. Jelinski SE, Yager JY, Juurlink BH. Preferential injury of oligodendroblasts by a short hypoxic–ischemic insult. Brain research. 1999;815(1):150–153.

36. Johnston MV, Hagberg H. Sex and the pathogenesis of cerebral palsy. Developmental Medicine & Child Neurology. 2007;49(1):74–78.

37. Khwaja O, Volpe JJ. Pathogenesis of cerebral white matter injury of prematurity. Archives of Disease in Childhood - Fetal and Neonatal Edition. 2007 Jul 18;93(2):F153–61.

38. Konfino T, Landa N, Ben-Mordechai T, Leor J. The Type of Injury Dictates the Mode of Repair in Neonatal and Adult Heart. Journal of the American Heart Association. 2015 Jan 27;4(1):e001320–e001320.

39. Kornack DR, Rakic P. Changes in cell-cycle kinetics during the development and evolution of primate neocortex. Proceedings of the National Academy of Sciences. 1998;95(3):1242–1246.

40. Kostovic I, Rakic P. Developmental history of the transient subplate zone in the visual and somatosensory cortex of the macaque monkey and human brain. Journal of Comparative Neurology. 1990;297(3):441–470.

41. Krägeloh-Mann I, Cans C. Cerebral palsy update. Brain and Development. 2009 Aug;31(7):537–44.

42. Krohn TC, Kornerup AH. The effects of and tolerances for Carbon Dioxide in relation to recent developments in laboratory animal housing Scand. J. Lab. Anim. Sci. No. 3. 2000. Vol. 27

43. Larouche A, Roy M, Kadhim H, Tsanaclis AM, Fortin D, Sébire G. Neuronal Injuries Induced by Perinatal Hypoxic-Ischemic Insults Are Potentiated by Prenatal Exposure to Lipopolysaccharide: Animal Model for Perinatally Acquired Encephalopathy. Developmental Neuroscience. 2005 Jul 19;27(2–4):134–42.

44. Larson BJ, Longaker MT, Lorenz HP. Scarless Fetal Wound Healing: A Basic Science Review: Plastic and Reconstructive Surgery. 2010 Oct;126(4):1172–80.

45. Lawn JE, Cousens S, Zupan J, Team LNSS, others. 4 million neonatal deaths: when? Where? Why? The lancet. 2005;365(9462):891–900.

46. Lee E-F, Jacobs RE, Dinov I, Leow A, Toga AW. Standard atlas space for C57BL/6J neonatal mouse brain. Anatomy and Embryology. 2005 Nov;210(4):245–63.

47. Lerch JP, Gazdzinski L, Germann J, Sled JG, Henkelman RM, Nieman BJ. Wanted dead or alive? The tradeoff between in-vivo versus ex-vivo MR brain imaging in the mouse. Frontiers in Neuroinformatics [Internet]. 2012 [cited 2016 Jun 27];6.

48. Libbin RPerson P. Neonatal rat surgery: avoiding maternal cannibalism. Science. 1979;206(4414):66-66.

49. Lövblad K-O, Laubach H-J, Baird AE, Curtin F, Schlaug G, Edelman RR, et al. Clinical experience with diffusion-weighted MR in patients with acute stroke. American Journal of Neuroradiology. 1998;19(6):1061–1066.

50. Malatesta P, Appolloni I, Calzolari F. Radial glia and neural stem cells. Cell and Tissue Research. 2008 Jan;331(1):165–78.

51. McQuillen PS, Ferriero DM. Perinatal subplate neuron injury: implications for cortical development and plasticity. Brain pathology. 2005;15(3):250–260.

52. McQuillen PS, Sheldon RA, Shatz CJ, Ferriero DM. Selective vulnerability of subplate neurons after early neonatal hypoxia-ischemia. The Journal of neuroscience. 2003;23(8):3308–3315.

53. McQuillen PS, Sheldon RA, Shatz CJ, Ferriero DM. Selective vulnerability of subplate neurons after early neonatal hypoxia-ischemia. The Journal of neuroscience. 2003;23(8):3308–3315.

54. Meng X, Fisher M, Shen Q, Sotak CH, Duong TQ. Characterizing the diffusion/perfusion mismatch in experimental focal cerebral ischemia. Annals of neurology. 2004;55(2):207–212.

55. Ment LR, Bada HS, Barnes P, Grant PE, Hirtz D, Papile LA, et al. Practice parameter: Neuroimaging of the neonate Report of the Quality Standards Subcommittee of the American Academy of Neurology and the Practice Committee of the Child Neurology Society. Neurology. 2002;58(12):1726–1738.

56. Mifsud G, Zammit C, Muscat R, Di Giovanni G, Valentino M. Oligodendrocyte Pathophysiology and Treatment Strategies in Cerebral Ischemia. CNS Neuroscience & Therapeutics. 2014 Jul;20(7):603–12.

57. Mori S, Zhang J. Principles of Diffusion Tensor Imaging and Its Applications to Basic Neuroscience Research. Neuron. 2006 Sep;51(5):527–39.

58. Moseley ME, Kucharczyk J, Mintorovitch J, et al. Diffusion-weighted MR imaging of acute stroke: correlation with T2-weighted and magnetic susceptibility-enhanced MR imaging in cats. AJNR Am J Neuroradiol1990;11:423-429

59. Nakajima W, Ishida A, Lange MS, Gabrielson KL, Wilson MA, Martin LJ, et al. Apoptosis has a prolonged role in the neurodegeneration after hypoxic ischemia in the newborn rat. The Journal of Neuroscience. 2000;20(21):7994–8004.

60. Neil JJ, Shiran SI, McKinstry RC, Schefft GL, Snyder AZ, Almli CR, et al. Normal brain in human newborns: apparent diffusion coefficient and diffusion anisotropy measured by using diffusion tensor MR imaging. Radiology. 1998;209(1):57–66.

61. Nijboer CHA, Kavelaars A, van Bel F, Heijnen CJ, Groenendaal F. Gender-Dependent Pathways of Hypoxia-Ischemia-Induced Cell Death and Neuroprotection in the Immature P3 Rat. Developmental Neuroscience. 2007;29(4–5):385–92.

62. Nishio S, CHEN Z-F, Yunoki M, Toyoda T, Anzivino M, Lee KS. Hypothermia-Induced Ischemic Tolerance. Annals of the New York Academy of Sciences. 1999;890(1):26–41.

63. Painter M. Animal models of perinatal asphyxia: Contributions, contradictions, clinical relevance. Seminars in Pediatric Neurology. 1995;2(1):37-56.

64. Perlman JM. Pathogenesis of hypoxic-ischemic brain injury. Journal of Perinatology. 2007 May;27:S39–46.

65. Petiet AE, Kaufman MH, Goddeeris MM, Brandenburg J, Elmore SA, Johnson GA. High-resolution magnetic resonance histology of the embryonic and neonatal mouse: a 4D atlas and morphologic database. Proceedings of the National Academy of Sciences. 2008;105(34):12331–12336.

66. Petschow R, Petschow D, Bartels R, Baumann R, Bartels H. Regulation of oxygen affinity in blood of fetal, newborn and adult mouse. Respiration Physiology. 1978;35(3):271-282.

67. Pimentel-Coelho PM, Michaud J-P, Rivest S. Evidence for a Gender-Specific Protective Role of Innate Immune Receptors in a Model of Perinatal Brain Injury. Journal of Neuroscience. 2013 Jul 10;33(28):11556–72.

68. Porrello ER, Mahmoud AI, Simpson E, Hill JA, Richardson JA, Olson EN, et al. Transient Regenerative Potential of the Neonatal Mouse Heart. Science. 2011 Feb 25;331(6020):1078–80.

69. Qiao M, Malisza KL, Del Bigio MR, Tuor UI. Transient Hypoxia-Ischemia in Rats: Changes in Diffusion-Sensitive MR Imaging Findings, Extracellular Space, and Na + -K + –Adenosine Triphosphatase and Cytochrome Oxidase Activity1. Radiology. 2002 Apr;223(1):65–75.

70. Ranasinghe S, Or G, Wang EY, Ievins A, McLean MA, Niell CM, et al. Reduced Cortical Activity Impairs Development and Plasticity after Neonatal Hypoxia Ischemia. Journal of Neuroscience. 2015 Aug 26;35(34):11946–59.

71. Rice JE, Vannucci RC, Brierley JB. The influence of immaturity on hypoxic-ischemic brain damage in the rat. Annals of neurology. 1981;9(2):131–141.

72. Robertson CFiner N. TERM INFANTS WITH HYPOXIC-ISCHEMIC ENCEPHALOPATHY: OUTCOME AT 3.5 YEARS. Developmental Medicine & Child Neurology. 2008;27(4):473-484.

73. Rosen GD, Sherman GF, Galaburda AM. Radial glia in the neocortex of adult rats: effects of neonatal brain injury. Developmental brain research. 1994;82(1–2):127–135.

74. Rumajogee P, Bregman T, Miller SP, Yager JY, Fehlings MG. Rodent Hypoxia–Ischemia Models for Cerebral Palsy Research: A Systematic Review. Frontiers in Neurology [Internet]. 2016 Apr 25 [cited 2016 Jun 27];7.

75. Rumpel, H., Nedelcu, J., Aguzzi, A., Martin, E., 1997. Late glial swelling after acute cerebral hypoxia–ischemia in the neonatal rat: a combined magnetic resonance and histochemical study. Pediatr. Res. 42, 54–59.

76. Samaiya PK, Krishnamurthy S. Characterization of mitochondrial bioenergetics in neonatal anoxic model of rats. Journal of Bioenergetics and Biomembranes. 2015 Jun;47(3):217–22.

77. Sasaoka N, Kawaguchi M, Kawaraguchi Y, Nakamura M, Konishi N, Patel H, et al. Isoflurane exerts a short-term but not a long-term preconditioning effect in neonatal rats exposed to a hypoxic-ischaemic neuronal injury: Preconditioning with isoflurane in neonatal rats. Acta Anaesthesiologica Scandinavica. 2009 Jan;53(1):46–54.

78. Scafidi J, Hammond TR, Scafidi S, Ritter J, Jablonska B, Roncal M, et al. Intranasal epidermal growth factor treatment rescues neonatal brain injury. Nature. 2013 Dec 25;506(7487):230–4.

79. Schmued LC, Stowers CC, Scallet AC, Xu L. Fluoro-Jade C results in ultra high resolution and contrast labeling of degenerating neurons. Brain Research. 2005 Feb;1035(1):24–31.

80. Semple BD, Blomgren K, Gimlin K, Ferriero DM, Noble-Haeusslein LJ. Brain development in rodents and humans: Identifying benchmarks of maturation and vulnerability to injury across species. Progress in Neurobiology. 2013 Jul;106–107:1–16.

81. Sharief AA, Johnson GA. EnhancedT2 contrast for MR histology of the mouse brain. Magnetic Resonance in Medicine. 2006 Oct;56(4):717–25.

82. Sheldon A, Chuai J, Ferriero D. A Rat Model for Hypoxic-Ischemic Brain Damage in Very Premature Infants. Neonatology. 1996;69(5):327-341.

83. Sheldon RA, Sedik C, Ferriero DM. Strain-related brain injury in neonatal mice subjected to hypoxia–ischemia. Brain research. 1998;810(1):114–122.

84. Shepherd TM, Thelwall PE, Stanisz GJ, Blackband SJ. Aldehyde fixative solutions alter the water relaxation and diffusion properties of nervous tissue. Magnetic Resonance in Medicine. 2009 Jul;62(1):26–34.

85. Singer D. Neonatal tolerance to hypoxia: a comparative-physiological approach. Comparative Biochemistry and Physiology Part A: Molecular & Integrative Physiology. 1999;123(3):221–234.

86. Sizonenko SV, Sirimanne E, Mayall Y, Gluckman PD, Inder T, Williams C. Selective Cortical Alteration after Hypoxic-Ischemic Injury in the Very Immature Rat Brain. Pediatric Research. 2003 Aug;54(2):263–9.

87. Sun S-W, Neil JJ, Liang H-F, He YY, Schmidt RE, Hsu CY, et al. Formalin fixation alters water diffusion coefficient magnitude but not anisotropy in infarcted brain. Magnetic Resonance in Medicine. 2005 Jun;53(6):1447–51.

88. Takada SH, Dos Santos Haemmerle CA, Motta-Teixeira LC, Machado-Nils AV, Lee VY, Takase LF, et al. Neonatal anoxia in rats: hippocampal cellular and subcellular changes related to cell death and spatial memory. Neuroscience. 2015;284:247–259.

89. Takada SH, Motta-Teixeira LC, Machado-Nils AV, Lee VY, Sampaio CA, Polli RS, et al. Impact of neonatal anoxia on adult rat hippocampal volume, neurogenesis and behavior. Behavioural Brain Research. 2016 Jan;296:331–8.

90. Takada SH, Sampaio CAG, Allemandi W, Ito PH, Takase LF, Nogueira MI. A modified rat model of neonatal anoxia: Development and evaluation by pulseoximetry, arterial gasometry and Fos immunoreactivity. Journal of Neuroscience Methods. 2011 May;198(1):62–9.

91. Ten VS, Wu EX, Tang H, Bradley-Moore M, Fedarau MV, Ratner VI, et al. Late Measures of Brain Injury After Neonatal Hypoxia-Ischemia in Mice. Stroke. 2004 Jul 8;35(9):2183–8.

92. Thoresen M. Who should we cool after perinatal asphyxia? Seminars in Fetal and Neonatal Medicine. 2015 Apr;20(2):66–71.

93. Towfighi J, Mauger D, Vannucci R, Vannucci S. Influence of age on the cerebral lesions in an immature rat model of cerebral hypoxia–ischemia: a light microscopic study. Developmental Brain Research. 1997;100(2):149-160.

94. Towfighi JYJ, Vannucci R. Influence of Mild Hypothermia on Hypoxic-Ischemic Brain Damage in the Immature Rat. 1993 [cited 2016 Jun 27];

95. Tuor U, Kozlowski P, Del Bigio M, Ramjiawan B, Su S, Malisza K et al. Diffusion- andT2-Weighted Increases in Magnetic Resonance Images of Immature Brain during Hypoxia–Ischemia: Transient Reversal Posthypoxia. Experimental Neurology. 1998;150(2):321-328.

96. Uehara H, Yoshioka H, Kawase S, Nagai H, Ohmae T, Hasegawa K et al. A new model of white matter injury in neonatal rats with bilateral carotid artery occlusion. Brain Research. 1999;837(1-2):213-220.

97. Van Everdingen KJ, Van der Grond J, Kappelle LJ, Ramos LMP, Mali W. Diffusion-weighted magnetic resonance imaging in acute stroke. Stroke. 1998;29(9):1783–1790.

98. Vannucci R, Connor J, Mauger D, Palmer C, Smith M, Towfighi J et al. Rat model of perinatal hypoxic-ischemic brain damage. J Neurosci Res. 1999;55(2):158-163.

99. Vannucci RC, Duffy TE. Carbohydrate metabolism in fetal and neonatal rat brain during anoxia and recovery. American Journal of Physiology–Legacy Content. 1976;230(5):1269–1275.

100. Vannucci RC, Perlman JM. Interventions for perinatal hypoxic–ischemic encephalopathy. Pediatrics. 1997;100(6):1004–1114.

101. Vannucci RC, Vannucci SJ. Perinatal Hypoxic-Ischemic Brain Damage: Evolution of an Animal Model. Developmental Neuroscience. 2005 Jul 19;27(2–4):81–6.

102. Vannucci RC. Experimental models of perinatal hypoxic-ischemic brain damage. APMIS Suppl.1993;40:89–95.

103. Vannucci SJ. Hypoxia-ischemia in the immature brain. Journal of Experimental Biology. 2004 Aug 15;207(18):3149–54.

104. Volpe JJ. Subplate Neurons-Missing Link in Brain Injury of the Premature Infant? PEDIATRICS Vol. 97 No. I January 1996

105. Wang S, Wu EX, Tam CN, Lau H-F, Cheung P-T, Khong P-L. Characterization of White Matter Injury in a Hypoxic-Ischemic Neonatal Rat Model by Diffusion Tensor MRI. Stroke. 2008 Aug 1;39(8):2348–53.

106. Wang WZ, Hoerder-Suabedissen A, Oeschger FM, Bayatti N, Ip BK, Lindsay S, et al. Subplate in the developing cortex of mouse and human: Subplate in the mouse and human. Journal of Anatomy. 2010 Oct;217(4):368–80.

107. Wendland MF, Faustino J, West T, Manabat C, Holtzman DM, Vexler ZS. Early Diffusion-Weighted MRI as a Predictor of Caspase-3 Activation After Hypoxic-Ischemic Insult in Neonatal Rodents. Stroke. 2008 Jun 1;39(6):1862–8.

108. Wood T, Osredkar D, Puchades M, Maes E, Falck M, Flatebø T, et al. Treatment temperature and insult severity influence the neuroprotective effects of therapeutic hypothermia. Scientific Reports. 2016 Mar 21;6:23430.

109. Yuen TJ, Silbereis JC, Griveau A, Chang SM, Daneman R, Fancy SPJ, et al. Oligodendrocyte-Encoded HIF Function Couples Postnatal Myelination and White Matter Angiogenesis. Cell. 2014 Jul;158(2):383–96.

110. Zhang J, Aggarwal M, Mori S. Structural insights into the rodent CNS via diffusion tensor imaging. Trends in Neurosciences. 2012 Jul;35(7):412–21.

111. Zucker R. Mouse hemoglobin during gestation Absence of fetal hemoglobin. Biochimica et Biophysica Acta (BBA) - Protein Structure and Molecular Enzymology. 1982;703(2):212-215.

112. Zupanc GKH, Sîrbulescu RF. Cell replacement therapy: Lessons from teleost fish. Experimental Neurology. 2015 Jan;263:272–6.

11 BIOGRAPHY

Gabriel Borden was born in Ithaca, NY, USA in 1968. He holds a bachelor's degree in physics from Cornell University (Ithaca, NY, USA, 1998). He completed a one year program in guitar performance at Musicians' Institute (Hollywood, CA, USA, 1990) and is a Microsoft Certified Systems Engineer.